

Submarine sliver in North Kona: A window into the early magmatic and growth history of Hualalai Volcano, Hawaii

Julia E. Hammer^{a,*}, Michelle L. Coombs^b, Patrick J. Shamberger^a, Jun-Ichi Kimura^c

^a Department of Geology and Geophysics, University of Hawaii, 1680 East-West Rd., Honolulu, HI 96822, United States

^b U.S. Geological Survey, 345 Middlefield Road MS 910, Menlo Park, CA 94025, United States

^c Department of Geoscience, Shimane University, Nishikawatsu 1060, Matsue 690-0853, Japan

Accepted 15 July 2005

Available online 4 January 2006

Abstract

Two manned submersible dives examined the Hualalai Northwest rift zone and an elongate ridge cresting at 3900 mbsl during a 2002 JAMSTEC cruise. The rift zone flank at dive site S690 (water depth 3412–2104 m) is draped by elongated and truncated pillow lavas. These olivine-rich tholeiitic lavas are compositionally indistinguishable from those examined further south along the bench, except that they span a wider range in dissolved sulfur content (200–1400 ppm). The elongate ridge investigated in dive S692, located at the base of the bench, is a package of distinct lithologic units containing volcanoclastic materials, glassy pillow breccias, and lava blocks; these units contain a range of compositions including tholeiitic basalt, transitional basalt, and hawaiite. The textures, compositions, and stratigraphic relationships of materials within the elongate ridge require that a variety of transport mechanisms juxtaposed materials from multiple eruptions into individual beds, compacted them into a coherent package of units, and brought the package to its present depth 10 km from the edge of the North Kona slump bench.

Sulfur-rich hawaiite glasses at the base of the elongate ridge may represent the first extant representatives of juvenile alkalic volcanism at Hualalai. They are geochemically distinct from shield tholeiite and post-shield alkalic magmas, but may be related to transitional basalt by high-pressure crystal fractionation of clinopyroxene. Tholeiitic glasses that compose the majority of the exposed outcrop are similar to Mauna Kea tholeiites and other Hualalai tholeiites, but they differ from younger basalts in having greater incompatible element enrichments and higher CaO for a given MgO. These differences could arise from small extents of partial melting during the transition from alkalic to shield stage magmatism. Low sulfur contents of most of the volcanoclastic tholeiites point to early emergence of Hualalai above sea level relative to the development of the mid-slope slump bench.

© 2005 Elsevier B.V. All rights reserved.

Keywords: ocean islands; basalt; hawaiite; sulfur; submarine landslide; geochemistry

1. Introduction

Interest in the processes affecting submarine flanks of Hawaiian volcanoes has grown in recent years, facilitated by improved bathymetric and backscatter

coverage (Smith et al., 2002) and intensification of manned submersible and remotely operated vehicle (ROV) operations in the region (e.g., Naka, 2002). Close inspection of submarine portions of the islands has revealed that edifice instabilities cause mass movements over a range of temporal and spatial scales (Lipman et al., 1988; Moore et al., 1989, 1994; Morgan et al., 2000), the more rapid of which have important implications for tsunami generation and thus hazards

* Corresponding author. Tel.: +1 808 956 5996; fax: +1 808 956 5512.

E-mail address: jhammer@hawaii.edu (J.E. Hammer).

throughout the Pacific ocean basin (Ward, 2001; McMurtry et al., 2004). There is also a growing appreciation for the role of mass movements in the growth, development, and destruction of ocean island volcanoes. Mass flows and magmatism are first order transformative processes that can occur simultaneously, perhaps in a feedback relationship (Presley et al., 1997; Lipman et al., 1988; Elsworth and Day, 1999). One or both of these processes continuously shape the subaerial and submarine portions of volcanoes. Mass flow deposits may also offer opportunities to examine the early stages of a volcano's history (e.g., Sisson et al., 2002) if they expose materials that do not outcrop elsewhere. For example, samples returned from submersible dives along Kīlauea's midslope bench in

1998–1999 revealed that diverse and strongly alkalic magmas erupted prior to relatively monotonous shield stage tholeiite at that volcano (Lipman et al., 2000, 2002), supporting the Hawaiian volcano paradigm of juvenile alkalic magmatism that was discovered at Lō'ihi (Moore et al., 1982; Frey and Clague, 1983). Lipman et al. (2002) suggested that submarine slopes morphologically similar to the Hilina slump could provide other opportunities to examine pre-shield magmatism. Accordingly, the midslope bench and elongate ridge in North Kona were identified as potential candidates for investigating Hualālai's early history.

In 2001 and 2002, the deep submarine portion of the North Kona region was explored and sampled for the first time during joint Japan–USA cruises, supported by

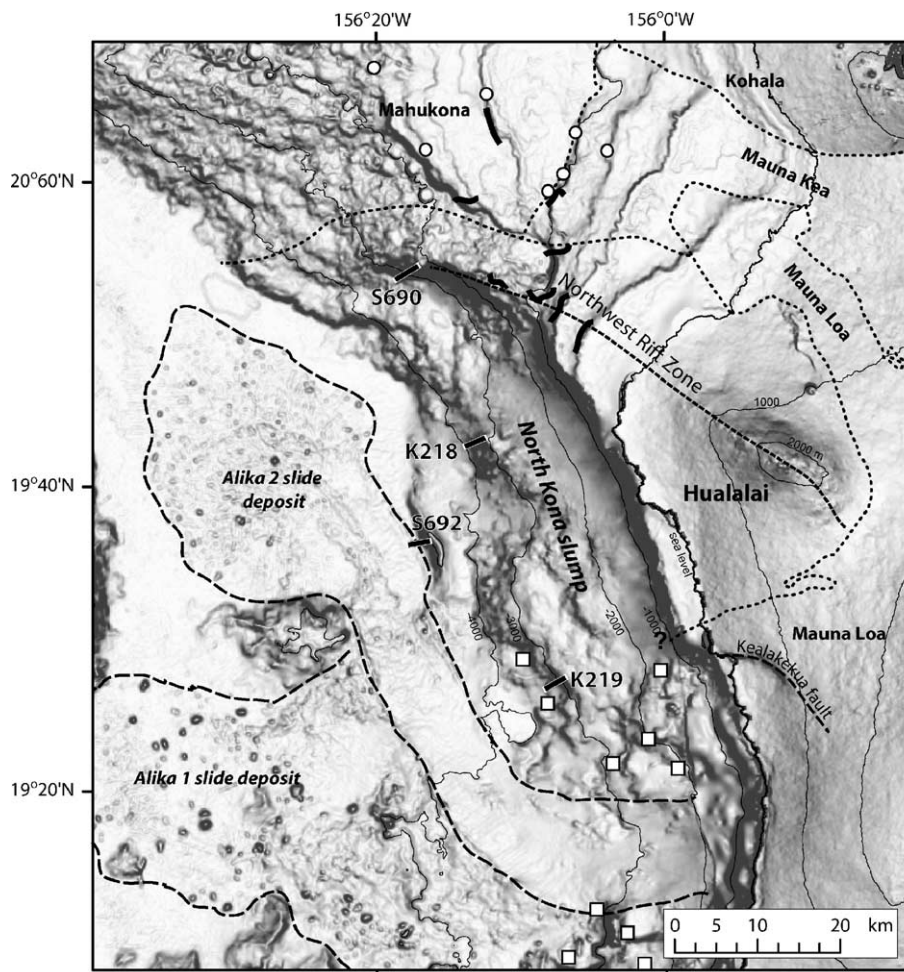


Fig. 1. Shaded slope map of the North Kona region, showing locations of *Shinkai 6500* and *Kaiko* dives (straight solid segments), *Pisces V* dives (thick curved segments on Māhukona and the Hualālai NW rift zone region), and dredges (squares=Davis et al., 2003; circles=Moore and Clague, 1992). Hualālai's rift zones are shown by heavy, short-dashed line. The submarine extension of the NW rift zone is approximate, and provided by Clague (2004, pers. comm.) Subaerial and submarine surficial contacts between separate volcanoes are shown by dotted lines and taken from Wolfe and Morris (1996) and Moore and Clague (1992), respectively. 1000 m contour intervals are shown as thin solid lines, with the sea level contour slightly heavier. The elongate ridge discussed in text is located at the site of dive S692.

the Japan Agency for Marine-Earth Science and Technology (JAMSTEC). The goals of this work were to compare landslide deposits in the region with others in the Hawaiian Islands, and to search for clues about the early geochemical and structural development of Hualālai Volcano. Four dive locations were selected along the steepest portions of Hualālai's flanks to maximize the probability that volcanic stratigraphy would be encountered (Fig. 1). In 2001, two dives using the remotely operated vehicle (ROV) *Kaiko* targeted the lower section of the North Kona slump bench (dives K218 and K219; Lipman and Coombs, 2006-this issue). In 2002, the manned submersible *Shinkai 6500* completed two additional dives on submarine Hualālai. Dive S690 investigated a steep section above the slump bench at its northern end nearest the volcano's northwest rift zone, and S692 explored the landward edge of the 'Ālika 2 landslide deposit originating from the west flank of Mauna Loa (Moore et al., 1989) and an adjacent elongate ridge below the central section of the North Kona bench (Fig. 1). All but the last *Shinkai* dive encountered in-place, compositionally homogeneous tholeiitic pillow lavas. The elongate ridge that was observed and sampled in S692 is composed of at least five distinct lithologic units, including glass sandstone, lava blocks, and glassy pillow breccia.

Here we present the results of a detailed study of lavas and volcanoclastic materials collected in the two *Shinkai* dives that can be used to infer a sequence of magmatic and erosional processes spanning an early shield stage of fractionated alkalic magmatism through the main shield stage of transitional and tholeiitic volcanism at Hualālai Volcano. The primary data include (1) submarine outcrop descriptions, hand sample and thin section petrography, and (2) major and trace element compositions of selected whole rocks and glasses. Our examination of the elongate sliver and slump scarp, in concert with other studies on Hualālai's west flank (Lipman and Coombs, 2006-this issue), is motivated by the need to fill in gaps of understanding about the submarine mass movements on Hualālai. For example, when did the flank begin to slip in relation to shield development? Was the volcano subaerial or still in deep water when the slump bench formed? What styles of landsliding operated on Hualālai's flanks? Hualālai is the sole historically active Hawaiian volcano that is in the post-shield stage of development. If the early history of the volcano can be inferred from a study of its deep submarine flanks, the geologic record for Hualālai will span a greater portion of the typical shield volcano's evolution than is currently available for any Hawaiian volcano.

2. Geologic setting

The Kona district of Hawai'i refers to the coast of the island extending from Kauna Point in the south to Kohala volcano in the north. The submarine region of North Kona lies directly offshore, bounded physiographically by the submarine extension of Hualālai northwest rift zone to the north, and to the south by the arcuate headwall source areas for the 'Ālika debris avalanches (Fig. 1). This region encompasses all of the submarine portion of Hualālai volcano, and probably the northernmost submarine flank of Mauna Loa; the contact between the two volcanoes is poorly defined below sea level.

Hualālai is the third youngest volcano on the island of Hawai'i, inferred to have started growing at ~800 ka and breached sea level at ~300 ka, based on analogy to other, better-dated Hawaiian volcanoes (Moore and Clague, 1992). The volcano's subaerial surface is covered by alkali basalt and trachyte lavas of the post-shield stage, although shield tholeiites have been recovered from water wells and from the volcano's submarine northwest rift zone (Moore et al., 1987). The end of shield building occurred at ~130 ka, based on the depth of the submarine-subaerial slope inflection along the submarine south rift (Moore and Clague, 1992). During Hualālai post-shield phase, the volcano initially erupted highly evolved trachytes from 114 to 92 ka (Cousens et al., 2003), followed by alkali basalt eruptions from 92 ka to the present (Moore et al., 1987).

Hualālai's northwest rift zone grew along the south flank of the now-submerged Māhukona Volcano and its northwest rift zone (Clague and Moore, 1991). The rift zone is cut by a steep scarp on its southern flank. Deep lobate terraces at the landward end of the ridge lie downslope from the scarp, which merge with similar terraces higher on the flanks of the volcanic edifice to the southeast. These benches have been mapped collectively as the North Kona slump (Moore et al., 1989, 1994). In this study, we follow Moore et al. (1989), using "landslide" to refer to any gravity driven mass movement, "slump" to refer to quasi-steady, incremental mass movement, and "debris avalanche" to denote catastrophic slope failure. The North Kona landslide has not been the focus of detailed study, perhaps because it is in relatively deep water and is not among the largest slumps in the Hawaiian Islands. Recent dives using the JAMSTEC ROV *Kaiko* on the main body of the slump show that it is obscured by draping tholeiitic pillow lavas (Lipman and Coombs, 2006-this issue).

In contrast with the North Kona slump, debris avalanches from Mauna Loa that formed the larger 'Ālika 1 and 2 deposits (Fig. 1) are very recent, energetic, and

Table 1
Observations, hand sample descriptions, and thin section petrography of samples collected on dive S692

Samples	Water depth (mbsl)	Lithology (unit no.)	Outcrop description [Fig. 3 video frame-grab]	Hand sample description	Petrography ^a	
					General description (componentry, sorting, angularity, mineralogy, etc.)	Alteration [Fig. 4 photomicrograph]
#1, 2	4510	'Alika2 levee basalt blocks	Landslide levee deposit: non-indurated, poorly sorted blocks	Aphyric dichtytaxitic basalt; #2 contains vesicles	97% groundmass (40% plagioclase, 45% pyroxene, 5% magnetite, 10% vesicles); microphenocrysts are olivine (20%), plagioclase (65%), clinopyroxene (14%) and orthopyroxene (tr)	Fresh interior, minor secondary minerals such as clays on surface
#3	4513	Talus blocks	No outcrop, floated block rests on top of sediment cover	Fresh, glass sandstone, zeolite-cemented (indurated); vitreous with 1 cm yellow rind and white vein material on exterior surfaces	Componentry: 60% angular glass fragments (points preserved), 28% clay or zeolite matrix, 9% mineral fragments, 3% basalt fragments; 95% of clasts in 75–1100 μm range, 68% between 350 and 800 μm , 1 mm thick vein of fine grained minerals (clay or zeolite) runs through section	Vesicles filled with low-birefringence bladed zeolites; fibrous zeolites infill between glass shards; uniform ~15 μm yellow rind on each fragment
#4, 5	4446, 4438	Muddy, cauliflower-textured breccia layer (1)	Knobby, friable, poorly indurated fragmental deposit forms flatiron "interfluves" [3F]	Friable lithic-rich muddy basalt breccia; brown-gray mottled color	#4: coherent but highly fractured basalt clast infilled by fine matrix material; cracks are puzzle-pieced. #5: glassy breccia, sparsely crystalline (5–10%); phenocrysts consist of faceted plagioclase (95%), olivine, and clinopyroxene	#4: gel-palagonite glass alteration pervasive. #5: gel-palagonite and fibro-palagonite glass alteration; zeolite infilling of vesicles and interstices; both samples: glass fragment interiors dark brown [sample #5: 4F]
#6	4419	Glass sandstone (2)	Collected at or near continuous white layer 20 cm thick at the contact between lithic breccia and indurated glass sandstone [3E]	Extremely altered glass-rich sandstone with slickensided zeolite mineralization and thin Mn_3O_4 coating	Texturally similar to other glassy sandstones (samples #7–10) in componentry, grain size and sorting; original glass shards angular to subangular (hydration rinds obscure angularity); no fabric or orientation of grains observed in three mutually perpendicular sections	No fresh glass remains, converted to fibro-palagonite; zeolites well developed between glass grains as radiating fibers [4E]
#7, 8, 9, 10	4405, 4404, 4403, 4383	Glass sandstone (2)	Heavily jointed, indurated, cliff-forming, massive deposit [3D]	Fresh, glass sandstone with 1 cm reddish alteration rind #7 contains slicken lines in zeolite on one surface	Componentry: 65% angular (points preserved), vesicular glass fragments, 20% clay or zeolite matrix, 10% mineral fragments, 5% basalt fragments; 95% of clasts in 30–2500 μm range, 68% between 200 and 500 μm ; multilithologic basalt fragments with fresh, euhedral olivine	Vesicles filled with low-birefringence bladed zeolites; fibrous zeolites infill between glass shards; uniform ~25 μm yellow rind on each fragment [sample #9: 4D]

#11, 12	4292, 4292	Breccia (3)	Jointed, buff-brown and black rounded blocks [3C] (talus shed from overlying, vertically jointed massive layer?)	11: olivine-rich breccia with fresh glass; 12: dense, picritic basalt with subordinate matrix; matrix is a veining material rich in basalt clasts and glass	#11: Large picrite fragment surrounded by glassy sand-sized fragments; matrix supported, where the matrix=50% glass, 30% olivine fragments, 20% fine grained material (clay or zeolite); basalt grains appear fractured in place. Fractures pass through glass shards and phenocrysts inside the glass shards. Many glass fragments contain spherical vesicles. #12: Basalt clasts surrounded by cemented picritic glass fragments; plagioclase and olivine phenocrysts; groundmass characterized by cruciform and skeletal Fe–Ti oxides	Very fresh: no alteration of glass, no secondary minerals such as zeolites or clay minerals [sample #12: 4C]
#13, 14, 15	4121, 4120, 4119	Basalt blocks (4)	Knobby, faintly bedded, ridge-forming, radially jointed outcrop [3B]	Dense olivine-basalt	13–15 v. similar; holocrystalline basalt blocks. 97% groundmass and 3% olivine phenocrysts. Groundmass contains radiating fibers of feldspar	Very fresh: no alteration, no secondary minerals such as zeolites or clay minerals [sample #14: 4B]
#16	3977	Float	Floated block in sediment	Vesicular, oxidized plag+ol basalt	Holocrystalline vesicular (~20%) basalt; elongate pyroxene and olivine phenocrysts in a fine-grained crystalline matrix; euhedral tabular groundmass plagioclase contrasts with samples #13–15	Very fresh: no alteration of glass, no secondary minerals such as zeolites or clay minerals
#17	3933	Fine volcanoclastic sediment (5)	Well-bedded, ledge-forming but poorly indurated, buff and black-colored siltstone [3A]	Unconsolidated, multicomponent volcanic glass siltstone	Angular fragments of heterogeneous lithologies dominantly in the 10–50 μm range. Components are ~40% basalt fragments, ~40% glass fragments, ~15% fine matrix, ~5% mineral fragments; unit rich in radiolarians	Very fresh: no alteration of glass, no secondary minerals such as zeolites or clay minerals [4A]

^a Mineral modes based on ≥ 300 points per thin section. Groundmass modes are approximate.

better understood (Lipman et al., 1988; McMurtry et al., 1999). Combined, the ‘Ālika events transported 200–800 km³ of debris more than 100 km from the western flank of that volcano in catastrophic failures (Moore et al., 1989). The ‘Ālika 2 event is a remarkable example of fluidized debris transport in a submarine setting. Apparently, the avalanche was deflected by the topography of the ‘Ālika 1 deposit, and was funneled northward between the flanks of Hualālai and a Cretaceous seamount, where it fanned out to form a lobate debris field at its terminus (Lipman et al., 1988).

2.1. Dive site selection

The two *Shinkai 6500* dive sites complement two *Kaiko* dives, K218 and K219, made in 2001, and investigate a data gap between Māhukona, sampled by numerous *Pisces V* dives and dredges (Moore and Clague, 1992), and dredges taken near the contact between Hualālai and Mauna Loa described by Davis et al. (2003). The *Kaiko* dives ascended the main body of the slump and encountered slope mantling, compositionally homogeneous tholeiitic pillow lavas that are interpreted to have erupted from Hualālai during its shield stage after emplacement of the slump (Lipman and Coombs, 2006–this issue). Dive S690 ascended the steep westernmost slope above the slump’s northern portion, a possible site for the headwall scarp for the slump. This site was deemed likely to reveal truncated (as opposed to draping) pillow lavas and provide a significant stratigraphic section through Hualālai’s northwest rift zone.

The site for Dive S692 was chosen to investigate both the levee of the ‘Ālika 2 deposit and a small (1.8 km × 8.2 km × 300–700 m high) sliver-shaped ridge landward of the ‘Ālika 2 deposit near its waist at the base of the North Kona slump (Fig. 1). The sliver’s size, its proximity to subaerial Hualālai (directly downslope from and 44 km to the west of the summit), its orientation parallel to the North Kona slump deposit, and its distance from the slump’s midslope bench (<10 km), strongly suggest that it is related to the growth and destabilization of Hualālai Volcano. Its position at the base of the slump, seaward of the *Kaiko* dive sites, as well as its smooth morphology, suggested that it escaped burial by lava flows.

3. Dive descriptions

3.1. Dive S690

Dive S690 ascended the headwall scarp of the North Kona slump from 3412 to 2104 mbsl. Pillow and sheet

lavas and talus were the only rock types observed during the dive, which can be summarized as consisting of five distinct sections with differing geology:

- (1) From the touchdown point to 3066 mbsl, the dive encountered heavily sedimented slopes with only occasional outcrops of pillow lavas; sample site 1 was a small pillow lava outcrop at 3064 mbsl.
- (2) From 3066 mbsl to 2534 mbsl, steep scarp-like outcrops of truncated pillow lavas, tens of meters high, alternated with lower angle sedimented slopes. During this interval, sampling was conducted at three sites (sites 2–4).
- (3) From 2534 to 2518 mbsl, an interval of shallow-dipping, intact, elongate pillow lavas was capped by sheet flows; the sample #5 site was in this interval.
- (4) From 2518 to 2114 mbsl, bottom morphology alternated between pillows and sediment-poor talus slopes; sample sites #6 and #7 were short steep pillow sections from this interval.
- (5) Finally, the slope lessened at 2114 mbsl, and flat, bulbous pillows and sheet flows predominated. On this flat surface, the ROV encountered the edge of a 20 m deep crater, the lateral extent of which is unknown. Sample #8 was taken from the interior of this feature.

At each of the eight sample sites, 2–4 rocks were taken from separate pillow lobes. Three of the samples broke into multiple fragments between collection and on-deck inventory, which introduced uncertainty into identifying their origins. For example, because of its similarity to compositions of site 7 glasses and known difficulties sorting out fragmented lavas, we infer that the sample named S690-3c was collected at site 7. (The original name is retained, but later reference to this sample assumes it was actually collected at the shallower site.) All of the samples are relatively fresh, with surficial chemical alteration limited to incipient palagonitization. Samples from sites 1–5 are olivine–plagioclase basalts and those from sites 6–8 are olivine-rich basalts to picrites.

3.2. Dive S692

Dive S692 began at the outer edge of the ‘Ālika 2 landslide deposit, 19°36.2110’N 156°17.7788’W, and collected 2 samples before traversing 1.3 km to the base of a steep (~45°) slope at the north end of the elongate ridge. Fifteen samples were collected as the submarine climbed 650 m up the side of the ridge to its point of

departure ~80 m below the crest. The dive traversed a total horizontal distance of ~3 km. Correlated descriptions of outcrop, hand samples, and thin sections collected from dive S692 are presented in Table 1. Fig. 2 summarizes the stratigraphic relationships, lithologies, magmatic affinities, and sulfur contents of all the samples analyzed. Key sampling locations depicting much of the outcrop-scale diversity in material coherence, bedding, alteration, jointing, and surface texture are shown in the video frame grabs of Fig. 3. Thin-section photomicrographs corresponding to each of the lithologies encountered in S692 are shown in Fig. 4. The panels of Figs. 3 and 4 are arranged stratigraphically; i.e., the deepest outcrops and samples are shown in the bottom panels (A and B), and the shallowest outcrops and samples are in the top panels (E and F). Moreover, samples in photomicrograph panels A–F of Fig. 4 are correlated as closely as possible to the sampling localities pictured in panels A–F of Fig. 3. Characteristics of the samples at the outcrop and thin section scales are summarized below in the sequence: lithology, alteration, whole-rock composition, and glass composition; details are provided in Table 1. Henceforth, dive S692 sample names are referenced by number (e.g., #11 for S692-11).

3.3. Dive S692 outcrops and lithologies

Two samples (#1 and #2) of the ‘Ālika 2 avalanche deposit were collected at 4510 mbsl from a low levee deposit of angular blocks and finer sediments. Both rocks are dense, aphanitic, holocrystalline basalt lavas lacking glass selvages. Neither has an Mn–Fe oxide coating, but the surface of #1 is dotted with sub-mm oxide patches, and #2 is partially altered to a buff-orange color.

A featureless, thickly sedimented plain ~1 km wide separates the debris avalanche levee from the elongate ridge. The first rocks encountered upon approaching the ridge comprise a talus apron at its base. One loose block from the outermost edge of the apron was collected (#3). It is petrographically similar to other indurated glass sandstones collected in place from the outcrop above it (samples #6–10; Table 1). The majority (~60% by height) of the ridge is covered by pelagic sediment, which obscures the underlying deposits. “Outcrop” is used here to describe all materials not obscured by sediment, and thus includes loose blocks as well as in-place stratigraphic horizons. Materials from in-place sedimentary units are called “bedrock”. The volcanoclastic materials that are exposed as bedrock on the

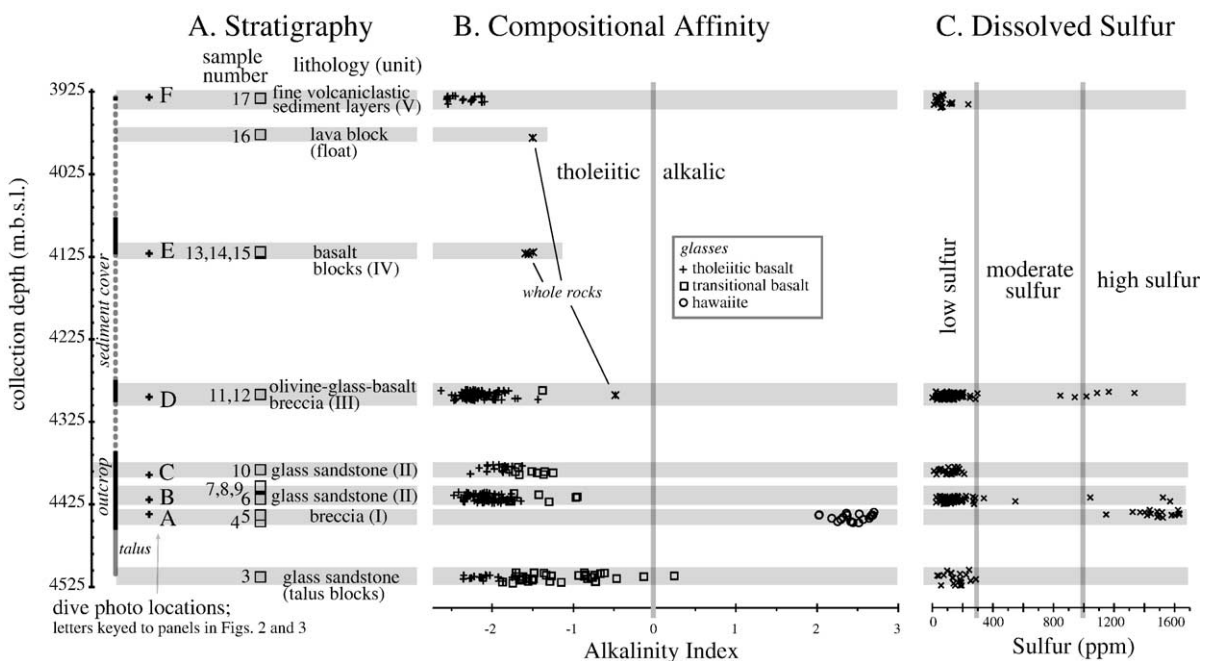


Fig. 2. (A) Stratigraphic locations of dive S692 photos (shown in Fig. 3) and sample collection sites (numbered boxes). (B) Sample lithologies, outcrop units (in parentheses), and alkalinity, defined as the shortest distance from the alkalic–tholeiitic dividing line of Macdonald and Katsura (1964). (C) Dissolved sulfur contents. Horizontal gray shaded bars guide the eye through individual samples and closely spaced groups of samples. The y-axis values (depths) of samples have been spread slightly in random fashion to show the distribution of x-values. Errors associated with analytical uncertainty and 1σ variation in major element and sulfur concentrations are smaller than the symbols.

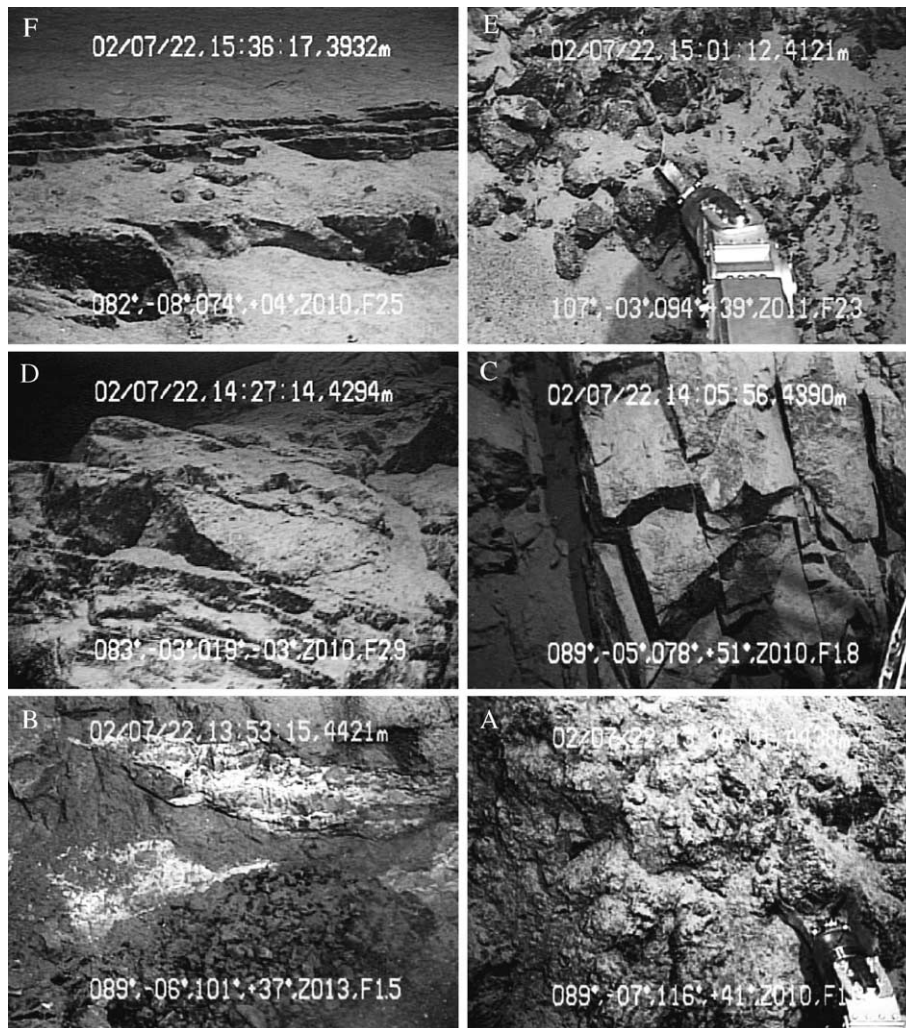


Fig. 3. Video frame grabs from dive S692 showing bedrock lithologic units discussed in text. Depth in mbsl is shown in upper right corner of each panel. The field of view is ~2 m across for all images except A, which is ~10 m across. (A) Unit V, bedded siltstone, site of sample #17, (B) unit IV, jumbled basaltic blocks, site of samples #13–15, (C) unit III, jointed pillow breccias, site of samples #11 and #12, (D) unit II, slabby, cliff-forming glass sandstone, site of samples #7–10, (E) base of unit II, intensely altered glass sandstone, site of sample #6, (F) unit I, cauliflower-textured glassy pillow breccia, site of samples #4 and #5.

ridge comprise the following lithologic units (Fig. 2), order from base to crest: (I) jumbled, cauliflower-textured alkalic glass and lithic pillow breccia; (II) bedded, landward-dipping, and variably altered tholeiitic and transitional basaltic glass sandstones; (III) pristine glass-rich olivine tholeiitic and transitional basalt breccia; (IV) dense olivine basalt lava block beds; and (V) layered, glassy (tholeiitic) volcanoclastic siltstone beds rich in radiolarians.

The cauliflower-textured breccia of unit I extends for 34 vertical meters above the talus apron and accounts for ~20% of the bedrock exposure (Fig. 3A). This material is deeply incised, with prominent hummocks resembling subaerial flatirons ~5 m wide extending

seaward from the ridge. Two samples of extremely friable material were taken from this section (#4 and #5). Both samples are clast-supported breccias composed of hawaiitic glass and basalt fragments. The maximum clast sizes of the samples are 2 and 5 cm, respectively. Sample #4 is composed of glassy pillow fragments with infilled crushed material (finer glass and basalt fragments) as matrix (Fig. 4A). Pillow fragments contain conspicuous euhedral plagioclase phenocrysts and Fe–Ti oxide stringers. Sample #5 is similar in texture, but contains no crystalline basalt. Rather, glass fragments are puzzle-pieced and in-filled by finely fragmented glass matrix and authigenic minerals (Fig. 4A). Clasts contain ~5 vol.% crystals, composed of

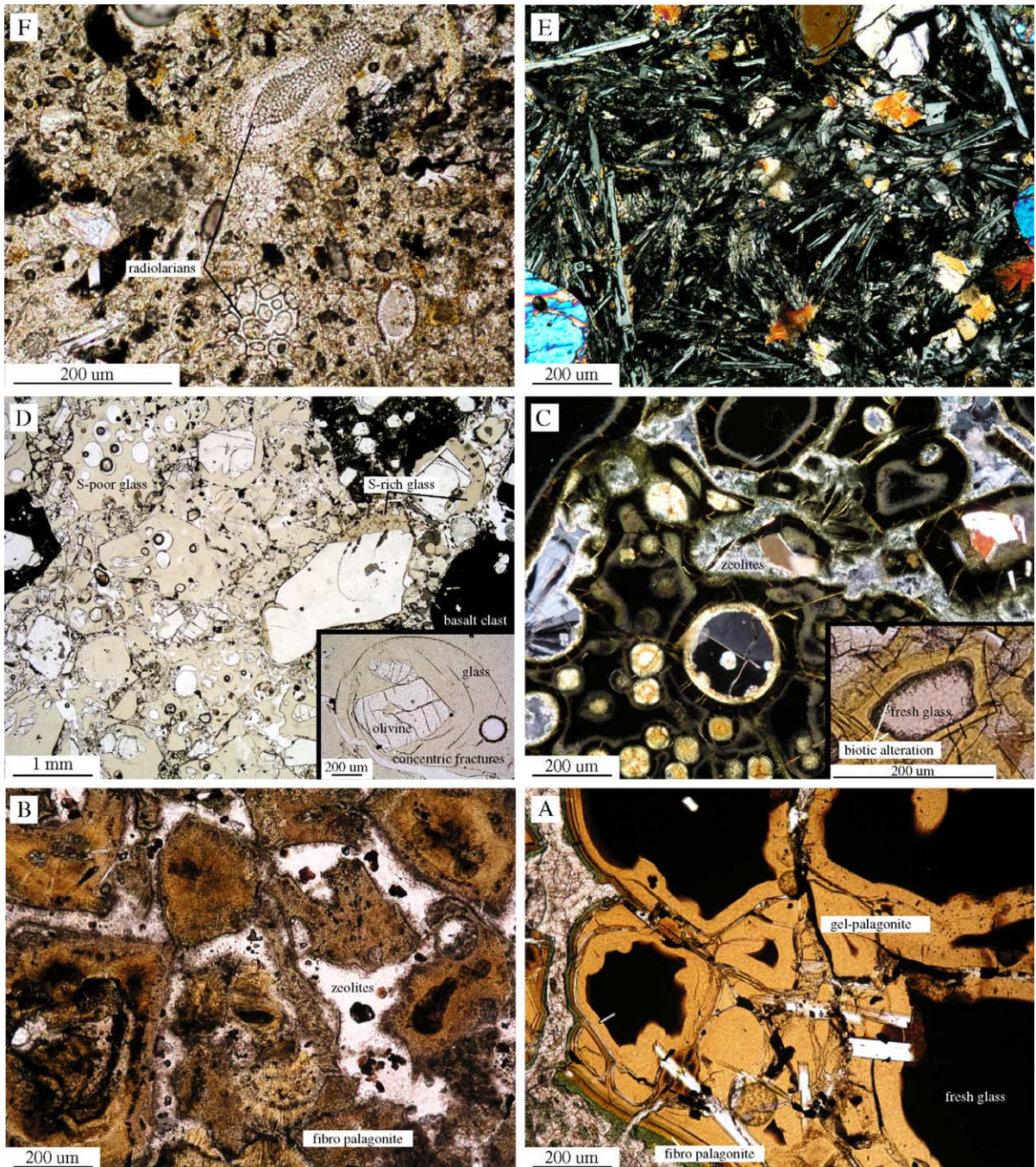


Fig. 4. Thin section photomicrographs of S692 dive samples. (A) Sample #17, (B) sample #14, (C) sample #12, (D) sample #10, inset #9, (E) sample #6, (F) sample #5. Images (A), (C), (E) and (F) are viewed in plane polarized light, (B) and (D) with crossed nicols. The 60 μm orange rinds visible in (A) are composed of an inner isotropic layer interpreted to be the amorphous form of palagonite (gel-palagonite), and a finely crystalline outer layer of fibro-palagonite. The former material yielded average microprobe totals of 77.0% and was depleted in SiO_2 , Al_2O_3 , MnO , Na_2O , and K_2O compared to fresh glass. The outer layer is a fine mixture of crystalline materials that may include various clay and zeolite minerals (Furnes et al., 2001). Outboard of the palagonite is a $\sim 16 \mu\text{m}$ thick layer of a platy green mineral, presumably clay, oriented such that basal cleavage is perpendicular to the shard surface tangents. Fragments of altered glass in the matrix of the breccia samples are similarly rimmed. The green mineral does not occur except in combination with palagonite as a glass alteration product. There is no fresh glass in sample #6 (B), whereas the cores of shards in overlying samples #7–10 (C) are unaltered. Pillow breccias (D) and the capping volcanoclastic siltstone (F) are devoid of authigenic minerals. Note the smooth spherical beads cored by olivine phenocrysts in (D). Stresses introduced in cooling pillow surfaces due to differences in the thermal expansion coefficients of olivine and the surrounding glass may have caused formation of the observed radial fractures as a form of elastic deformation (Ryan, 1979). Lava blocks are holocrystalline and fresh (E). (For interpretation of the references to color in this figure legend, the reader is referred to the web version of this article.)

euhedral plagioclase laths, Fe–Ti oxides, olivine phenocrysts, and clinopyroxene in order of decreasing abundance.

The zeolite-cemented glass sandstone of lithologic unit II was the dominant rock type collected during the dive, comprising one third of the samples (#6–10). This cliff-forming lithology, which makes up only 10% of the vertical height of the ridge but ~35% of the exposed bedrock (Fig. 2), may be disproportionately represented in the sample set with respect to its presence in the ridge. The unit is relatively hard compared to others, and is characterized by a prominent joint set with spacing 30–50 cm (Fig. 3C). All of the samples of this unit are composed of angular to subangular fragments and are similar in componentry, grain size distribution, and sorting. The few rounded glass grains that are present in these samples (e.g., Fig. 4D) may not have been mechanically abraded (e.g., Fig. 4D inset).

All of the glass fragments in these samples are somewhat chemically altered (Fig. 4C), and correspond to various stages of palagonitic alteration as described by Schiffman and Walton (2003). However, the intensity of chemical alteration increases markedly within a 10 m interval at the base of the exposed outcrop. A laterally continuous, irregular (0–1 m thick) band of white rocks at the boundary between units I and II, interpreted as a zone of intense alteration (Fig. 3B), corresponds to pervasive glass palagonitization and interstitial mineralization of sample #6 (Fig. 4B).

Unit III includes subhorizontally landward dipping beds (Fig. 3D), an overlying jumble deposit of cobble to block-sized clasts, and an irregularly jointed spine rising ~2 m above. Samples #11 and #12 were taken from the block bed, in the middle of this section. This unit represents only 16% of bedrock height, but the two breccia samples from it are more texturally diverse than the four glass sandstones analyzed from unit II. Sample #11 consists of a 4 cm holocrystalline basalt fragment surrounded by rounded grains of dense, olivine-rich glass (≤ 1.5 mm) in a matrix of angular glass fragments, cemented by zeolites. Sample #12 is a single olivine basalt fragment enclosing an enclave of crystal-rich glass fragments and smaller basalt clasts, with no discernible cementing mineral. This sample is less mechanically weathered than #11, having vesicular, puzzle-pieced picritic glass fragments (up to 1 cm) that are uniformly angular (Fig. 4D). The glasses in both #11 and #12 are conspicuously fresh (i.e., no palagonite rinds), and both contain angular puzzle-pieced fractures in the glass between basalt clasts. These characteristics are similar to the incipient and early smectitic stages of Schiffman and Walton (2003).

Unit IV, from which lava samples #13–15 were collected, is a jumble of block-sized lava clasts coated with a thin layer of pelagic sediment (Fig. 3E). Curved fractures within large clasts are evocative of pillow surfaces, but the overall outcrop characteristics do not include characteristics of a primary lava flow or pillow field, and the blocks do not have glass rinds. The sample site is a wedge-shaped interfluvial perpendicular to the elongate ridge. This unit represents 26% of the bedrock height. The samples from it are relatively fresh, fine-grained dense holocrystalline olivine basalt (Fig. 4E). Lava sample #16, collected from float above unit IV, is striking by contrast: it is vesicular, oxidized on the exterior, and contains a coarser groundmass of euhedral tabular plagioclase.

The uppermost lithologic unit observed in the elongate ridge is a finely bedded sequence of unconsolidated volcanoclastic sediment layers. The beds dip landward slightly ($\leq 5^\circ$) and most range between 50 cm and 2 m thick (Fig. 3F). Unit V comprises only 2% of the bedrock height and $\leq 1\%$ of the overall ridge. The materials in this unit are distinct from the other volcanoclastic units in being finer grained, poorly sorted, poorer in glass, multilithologic, and fossiliferous (Fig. 4F; Table 1).

4. Petrography, petrology, and geochemistry

4.1. Dive S692 alteration and secondary mineralization

As summarized above and in Table 1, the intensity and pervasiveness of chemical alteration in the volcanoclastic materials vary significantly. All samples collected from the lower ~100 m of the ridge (units I and II) are somewhat altered, while the overlying deposits contain pristine glass and less authigenic mineralization within the matrix and cracks. Chemical weathering and secondary mineralization of these lower units, as assessed from hand sample descriptions, thin section petrography, and XRD analyses are quite variable.

The dark brown glass fragments in sample #4 are rimmed by 0–0.2 mm of pale yellow gel-palagonite. The glass fragments in breccia samples #5 are tri-colored, having dark brown cores, thick orange rinds, and thin green outer rims. The cores of samples #4 and #5 are fresh glass, as determined by microprobe analysis; the analytical totals average 99.1% (Table 3). Fresh, high-S alkalic glasses collected elsewhere from submarine Hawaiian sections share this characteristic coloration (e.g., Coombs et al., 2004b). Alteration rinds are associated with breccia cracks and fragment margins, indicating that alteration took place after brecciation.

Unit II is quite diverse in terms of alteration features. Most of the change in extent of chemical alteration

occurs between samples collected only ~20 vertical m apart (#6 and #7). There is no fresh glass remaining in sample #6. It is the most extensively altered sample collected on dive S692, and is closely correlated in outcrop with an irregular white layer that was obvious from the submersible and captured on video (Fig. 3B). Abrasion of the outcrop during sampling uncovered even more highly reflective (whiter) material below. Thus, the boundaries of the white layer as seen in the video probably have more to do with recent spallation activity than actual variations in the extent of bedrock alteration. Sample #6 is greenish-gray in hand specimen, and has a 1-mm glass-poor, planar layer of very fine authigenic minerals on one side. Glass fragments within the sample appear to be thoroughly converted to fibro-palagonite (Fig. 4E), and are rimmed by spherical fibrous aggregates. Samples #7–10 are roughly similar in

alteration characteristics, although only sample #7 has a slickensided layer of white authigenic minerals on one side (~1 mm thick). Orange rinds of gel-palagonite on the glass fragments in these samples are thin relative to the average fragment radii (~10%). Rinds penetrate equal distances on all edges and are roughly equivalent on all clasts. Where fragment edges meet in acute angles, the palagonite equipenetration surface softens the points and gives a false impression of grain rounding as viewed in plane-polarized transmitted light. Cross-polarized light accentuates the difference between isotropic (fresh glass and gel-palagonite) and anisotropic (authigenic minerals and fibro-palagonite) materials (Fig. 4D), and shows that the true grain edges are angular to sub-angular. Biotically generated tubular type alteration (Furnes et al., 2001) is apparent at the interface between fresh cores and palagonite rims (Fig. 4D, inset).

Table 2
Whole rock compositions of dive S692 lavas

‘Ālika 2 lava blocks			Elongated ridge				
Sample	s692_1	s692_2	s692_12 ^a	s692_13	s692_14	s692_15	s692_16
Type	atb	tb	tb	tb	tb	tb	ptb
SiO ₂	50.8	51.0	44.5	49.6	49.4	49.7	48.2
TiO ₂	2.56	2.27	1.32	1.96	1.83	1.89	1.37
Al ₂ O ₃	13.2	13.6	7.8	12.9	12.0	12.5	10.2
Fe ₂ O ₃	12.9	12.1	12.7	11.4	12	11.9	12.3
MnO	0.17	0.17	0.17	0.15	0.17	0.17	0.17
MgO	6.07	6.61	23.2	9.26	12.4	11.1	17.9
CaO	9.9	10.3	6.34	10.3	9.55	9.91	7.87
Na ₂ O	2.51	2.43	1.33	2.11	1.93	2.02	1.68
K ₂ O	0.45	0.32	0.22	0.49	0.37	0.35	0.23
P ₂ O ₅	0.29	0.25	0.19	0.23	0.21	0.22	0.18
LOI	0.90	0.65	1.66	1.25	0.32	0.20	–0.33
Total wt.%	98.9	99.1	97.8	98.4	99.9	99.8	100.1
<i>XRF (values in ppm)</i>							
V	352	325	198	300	286	299	215
Cr	105	171	1510	504	754	766	827
Ni	81	71	1210	245	436	373	865
Cu	162	131	83	127	105	127	98
Zn	104	96	101	97	94	101	94
Ga	15	19	11	17	12	19	13
Mo	3	3	2	<2	2	3	<2
Rb	10	3	3	7	6	5	4
Sr	293	289	200	280	260	266	205
Y	30	28	15	23	21	22	17
Zr	153	133	74	114	101	107	78
Nb	11	10	8	10	9	10	7
Ba	80	69	44	69	67	72	49
La	11	12	11	11	10	11	8
Ce	25	26	19	24	22	22	18
Nd	<10	11	<10	<10	<10	<10	<10

Type: atb—aphyric tholeiitic basalt, tb—olivine phyric basalt (including picrite), ptb—olivine-plagioclase basalt.

Concentrations of Ge, As, Se, Ag, Cd, Sn, Sb, W, Bi, Cs, Pb, Th, U, and Br are below the minimum detection limit (typically 3 ppm) in every sample.

^a Basalt clast within breccia.

Powders of samples #6–10 were analyzed by X-ray diffraction at the University of Hawaii using a Scintag PAD V powder X-ray diffractometer at standard operating conditions (scan speed 1° min^{-1} using Cu $K\alpha$ radiation, scanning over $4\text{--}45^\circ 2\theta$). Peaks corresponding to lattice d-spacings of the zeolite analcime were present in the spectrum for sample #6. The spectra obtained for samples #7–10 all indicate the presence of the zeolites chabazite and phillipsite, with no analcime peaks. The formation conditions of these zeolites overlap significantly, making it impossible to determine with confidence the temperature at which these minerals formed, but analcime is stable to higher temperatures ($75\text{--}300^\circ \text{C}$) than chabazite ($0\text{--}75^\circ \text{C}$) in hydrothermally altered Icelandic basalt (Chipera and Apps, 2001). Its presence in sample #6 and conspicuous absence from samples #7–10 is consistent with the on-site observations that chemical alteration intensified toward the base of unit II where #6 was collected.

4.2. Dive S692 XRF whole rock analysis

Whole rock compositions for seven samples from dive S692 were determined at the USGS in Denver, Colorado. Samples were trimmed to remove visible

weathering rinds, followed by grinding to remove saw marks. Samples were then washed in deionized water in an ultrasonic bath, dried, crushed, and powdered in an alumina shatterbox. Major element oxide and trace element abundances were determined by wavelength-dispersive and energy-dispersive XRF, respectively, by D. Siems, using techniques outlined in Taggart et al. (1987) and Siems (2000).

All analyzed samples are tholeiitic basalts (Table 2). Samples #1 and #2, from the 'Ālika 2 slide deposit, are compositionally similar, with relatively high SiO_2 and low MgO reflecting their olivine-poor character (Table 2). They plot within trends typical of Hawaiian tholeiite (e.g., compare with Mauna Loa lavas on a total-alkali silica diagram, Fig. 5). They also have trace element ratios thought to be characteristic of Mauna Loa lavas. For example, they have Zr/Nb ratios of 14 and 13, which overlap with those of Mauna Loa lavas (Frey and Rhodes, 1993; Sisson et al., 2002) (Table 2).

From the elongate sliver, sample #12 has high MgO and low SiO_2 content that reflects its olivine-rich nature. Samples #13, #14, and #15, all collected from unit IV, are compositionally similar and suggest that the unit is monolithologic. Finally, #16, a loose lava block near the top of the ridge, is relatively MgO-rich, intermedi-

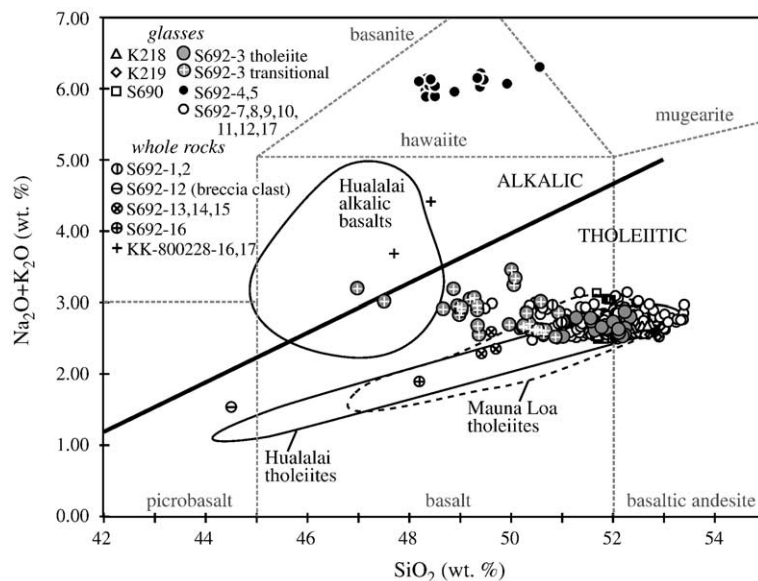


Fig. 5. Total alkalis versus silica diagram showing the tholeiite-alkalic affinity dividing line (Macdonald and Katsura, 1964). *Kaiko* glass data from Lipman and Coombs (2006-this issue), "KK-" samples are glasses collected from the 'Ālika 2 debris lobe, interpreted to have originated from Hualālai (McMurtry et al., 1999), S690 and S692 are data from this study (Tables 2 and 3). For the new data, each symbol represents the average of at least three analyses if a glass shard or 4–10 analyses if a pillow selvage. Typical 2σ variation of replicate analyses is within the symbol size. Labeled fields enclose 95% of the Hualālai and Mauna Loa whole rock and glass analyses (cited in text). The number of analyses represented by the fields labeled Hualālai alkalic basalts, Hualālai tholeiites, and Mauna Loa tholeiite fields are 295, 91, and 753, respectively. The whole rock/glass proportions differ among these data sets: 95%, 50%, and 21% of the Hualālai alkalic data, Hualālai tholeiite data, and Mauna Loa data are whole rocks, respectively.

ate between samples #12 and #13–15. In contrast to the high Zr/Nb of samples #1 and #2, Zr/Nb ratios for rocks from the elongate sliver range from 9 to 11.

4.3. EMP glass analysis

Glasses from both dives were analyzed using the Cameca SX-50 Electron Microprobe (EMP) at the University of Hawaii at Manoa. In volcanoclastic samples, 25–50 grains per thin section were analyzed in triplicate. Pillow selvages were analyzed at 5–10 spots per sample. Analytical conditions included an accelerating voltage of 15 kV and a 10 or 15 nA beam, defocused ($\geq 10 \mu\text{m}$) to minimize alkali loss. Na was counted first for 20 s. Peak count times for other elements ranged from 30–60 s. Major elements were calibrated on

Smithsonian standards Makaopuhi Lava Lake glass, A99 (Mg, Si, Ti, and Fe), Juan de Fuca glass, VG-2 (Na, Al, and Ca), and Yellowstone rhyolite glass, VG568 (K). Mn and P were calibrated on Verma garnet and Smithsonian apatite standards respectively. Sulfur was analyzed simultaneously with major elements, using 60-s count intervals on the peak and 25 s off-peak. S was calibrated on a troilite (FeS) standard from the Staunton Meteorite. Reported concentrations are calculated using ZAF-PAP procedures (Reed, 1993). Instrument drift outside analytical precision was monitored by repeatedly analyzing VG-2 and A99 to derive nominal correction factors that were applied to sample analyses.

Major element and sulfur plots (Figs. 5–7) of glass data for dives S690 and S692 include analyses from

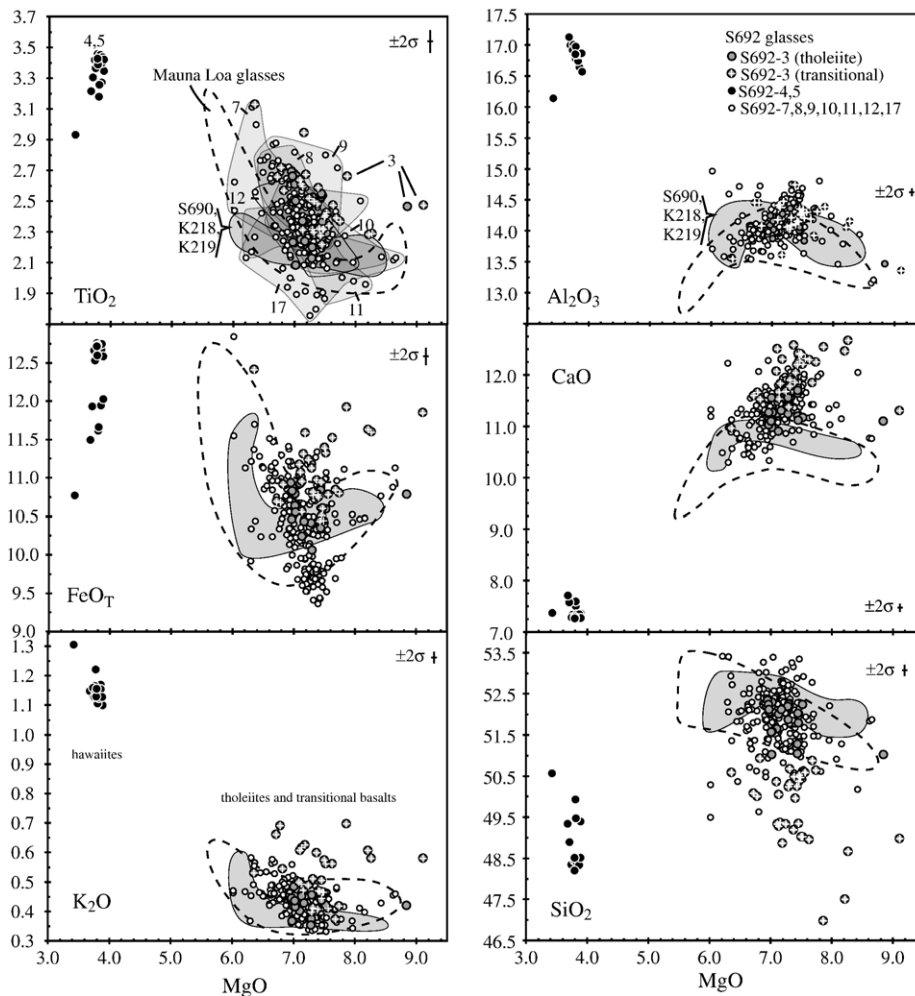


Fig. 6. MgO-oxide variation diagrams for basalt and hawaiite glasses recovered in dives K218, K219, S690, and S692 shown with the field representing Mauna Loa (described in Fig. 5 caption) glasses. First panel (TiO₂ diagram) shows the fields bounding analyses from each sample in dive S692; these field lines are omitted for clarity in subsequent panels. Shaded fields in other panels enclose K218, K219, and S690 tholeiite glasses. Error bars are 2σ variation in replicate analyses of S692 glasses.

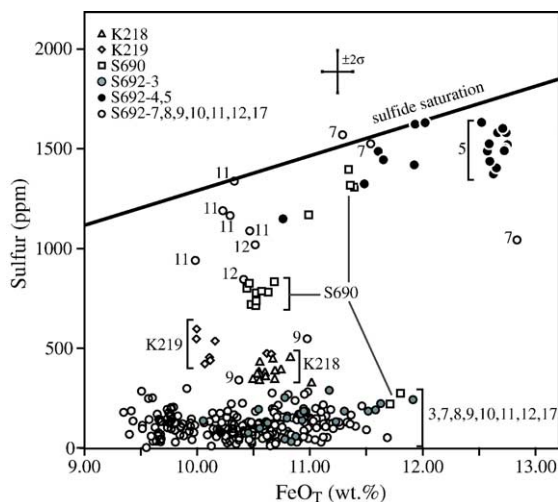


Fig. 7. Variation of dissolved sulfur concentrations with glass FeO_T . The sulfide saturation curve represents the locus of points formed by MORB glasses in pyrrhotite-bearing samples (Wallace and Carmichael, 1992); it is shown as an approximate upper limit to dissolved S in basalts. Symbols are as defined in previous figures. Numerical labels beside moderately to high-S points are S692 sample numbers.

other JAMSTEC dives in the North Kona region (Lipman and Coombs, 2006-this issue), as well as previously published Hualālai data. The latter are composed of three glass and whole-rock series: Hualālai alkalic lavas (Yoder and Tilley, 1962; Tatsumoto, 1966; Macdonald, 1968; Roeder and Emslie, 1970; Clague et al., 1980; Anonymous, 1981; Moore, 1987; Moore and Clague, 1987; Moore et al., 1987; Rhodes and Hart, 1995; Sims et al., 1999; Kauahikaua et al., 2002), Hualālai tholeiitic lavas (Moore et al., 1987; Garcia et al., 1989; Moore and Clague, 1992; Norman and Garcia, 1999), and tholeiites from Mauna Loa (Moore and Clague, 1987, 1992; Moore et al., 1987; Bohrsen and Clague, 1988; Rhodes and Vollinger, 2004).

4.3.1. Dive S690 major elements

Approximately half of the 29 lava samples collected on dive S690 had glass selvages suitable for analysis by EMP (Table 3). Multiple lava samples from a single site (named S690-5a, 5b, 5c, etc.) have oxide contents that are identical within analytical error. All of these compositions are similar to previously studied Hualālai submarine tholeiites (e.g., K218 and K219 lavas; Lipman and Coombs, 2006-this issue) in terms of total alkalis versus silica (e.g., plotting beneath a dense cluster of points in Fig. 5), and their trends on MgO variation diagrams (e.g., Fig. 6). The compositions of S690 selva glasses fall into two clusters that correspond to collection depth. Samples collected between 3002 and 2520 mbsl have similar compositions (e.g.,

6.03–6.30 wt.% MgO), whereas those collected between 2445 and 2104 m have equally uniform but distinct compositions (e.g., 8.19–8.40 wt.% MgO).

4.3.2. Dive S692 major elements

The pillow breccias from unit I of dive S692 are classified as hawaiites (Fig. 5) by their high proportion of Na_2O to K_2O (Le Maitre, 2002). They appear to be the most alkalic of any mafic magmas yet sampled from Hualālai. For comparison, the only Hualālai magmas yet encountered that are richer in alkalis are trachytes (~62 wt.% SiO_2 and ~6 wt.% total alkalis), erupted subaerially at the beginning of the post-shield stage (Cousens et al., 2003). All other samples retrieved during dives S692 are, like those of K218, K219, and S690, tholeiitic basalts and basaltic andesites according to the Irvine and Baragar (1971) and Macdonald and Katsura (1964) classification schemes (Fig. 5). Following Sisson et al. (2002), transitional tholeiites are distinguished in figures and tables from normal tholeiitic basalt as having <51.0 wt.% SiO_2 and >2.5 wt.% total alkalis ($\text{K}_2\text{O} + \text{Na}_2\text{O}$).

The glasses of samples collected from units I, II, and III on dive S692 are shown in MgO-oxide variation diagrams with fields representing tholeiites from Hualālai (dives S690, K218 and K219) and Mauna Loa (Fig. 6). Several geochemical features are striking. First, the tholeiitic glass fragments within individual sandstone samples are heterogeneous (e.g., TiO_2 ; Fig. 6A, Table 3), and do not share a single plausible crystal fractionation trend. By comparison with the ongoing Kīlauea eruption (Garcia et al., 1992; Thornber et al., 2003), the glass compositions in these samples are too varied to have originated in single eruptive episodes. Sample #3 contains a particularly wide variety of glass compositions, generally with lower SiO_2 , and greater TiO_2 , FeO_T , Na_2O , and K_2O than other S692 tholeiite glasses. The sample #3 compositions extend out of the narrow, positively sloping tholeiitic fields defined by prior analyses of Hualālai magmas, and several fall within the cloud of analyses representing Hualālai alkalic basalts (Fig. 5). These glasses are similar in composition to transitional basalts found at Lō'ihi (Moore et al., 1982; Garcia et al., 1993, 1995; Clague et al., 2000), Māhukona (Clague and Moore, 1991) and pre-shield Kīlauea (Lipman et al., 2002; Sisson et al., 2002). Finally, there is extensive overlap of the S692 samples with previously published Hualālai and Mauna Loa tholeiite analyses in the 50–53 wt.% SiO_2 range (Fig. 5), but the S692 glasses do not follow the same broad MgO-variation trends as these tholeiites (Fig. 6). They differ in having markedly greater CaO for a given

Table 3
Representative electron microprobe analyses of dives S690 and S692 glasses

	<i>n</i> ^a	SiO ₂	TiO ₂	Al ₂ O ₃	FeO _T	MnO	MgO	CaO	Na ₂ O	K ₂ O	P ₂ O ₅	S (ppm)	Oxide total (wt.%)	
Dive S690														
<i>Tholeiitic basalt (tb) and picrite (tp) pillow lavas</i> ^b														
s690_2c	tb	8	51.9	2.39	14.1	11.35	0.17	6.14	10.42	2.52	0.51	0.28	1400	99.9
s690_3a	tb	5	52.0	2.43	14.1	11.40	0.16	6.13	10.40	2.50	0.53	0.28	1300	100.0
s690_3d	tb	7	51.7	2.34	14.1	11.37	0.17	6.03	10.25	2.62	0.52	0.28	1300	99.5
s690_4b	tb	8	51.9	2.21	14.0	11.00	0.17	6.25	10.31	2.55	0.49	0.27	1150	99.3
s690_5a	tb	6	52.1	2.29	13.5	11.72	0.19	6.25	10.66	2.34	0.33	0.21	200	99.7
s690_5b	tb	7	52.4	2.33	13.5	11.81	0.18	6.30	10.64	2.35	0.33	0.21	250	100.1
s690_6a	tp	7	51.7	2.05	13.7	10.48	0.16	8.24	10.49	2.23	0.30	0.18	700	99.6
s690_6c	tp	7	51.8	2.06	13.7	10.53	0.16	8.25	10.60	2.19	0.30	0.18	700	99.9
s690_6d	tb	7	51.7	2.07	13.7	10.45	0.17	8.29	10.50	2.19	0.30	0.17	800	99.6
s690_6e	tp	7	52.0	2.00	13.8	10.53	0.15	8.19	10.53	2.28	0.30	0.17	800	100.0
s690_7a	tp	7	52.1	2.13	13.8	10.64	0.17	8.37	10.59	2.24	0.31	0.19	800	100.7
s690_7b	tb	8	52.1	2.14	14.0	10.47	0.17	7.40	10.89	2.27	0.31	0.20	800	100.1
s690_3c ^b	tp	5	51.6	2.08	13.8	10.69	0.15	8.34	10.54	2.25	0.31	0.21	850	100.1
s690_8a	tp	10	52.0	2.06	13.7	10.53	0.17	8.40	10.53	2.22	0.30	0.21	750	100.2
s690_8b	tb	9	52.2	2.09	13.6	10.58	0.16	8.39	10.59	2.22	0.32	0.19	800	100.4
Dive S692														
<i>Sample #3: glass sandstone, tholeiitic to transitional</i> ^c (<i>tr</i>) basalt [51] ^d														
s692_3d	tr	5	50.6	2.34	14.3	10.78	0.16	7.56	12.32	2.27	0.36	0.21	N.A.	100.9
s692_3e		5	52.3	2.50	14.2	10.63	0.16	7.03	10.97	2.36	0.40	0.21	150	100.8
s692_3f	tr	3	49.2	2.48	14.7	10.97	0.19	7.38	12.58	2.50	0.55	0.25	200	100.8
s692_3g	tr	5	48.7	2.29	14.2	11.60	0.19	8.27	12.67	2.38	0.53	0.25	N.A.	101.0
s692_3h	tr	3	50.6	3.13	13.5	12.41	0.19	6.36	10.96	2.53	0.48	0.29	N.A.	100.5
s692_3h1	tr	3	50.6	2.37	14.3	10.80	0.17	7.74	12.25	2.19	0.37	0.19	150	101.0
s692_3i		5	52.0	2.53	14.1	10.35	0.17	7.44	11.19	2.32	0.39	0.23	N.A.	100.8
s692_3j		3	51.3	2.54	14.0	10.88	0.15	7.44	11.64	2.39	0.40	0.24	50	101.0
s692_3l		3	52.3	2.69	14.1	10.94	0.16	6.95	11.05	2.41	0.39	0.22	150	101.2
s692_3m		3	51.9	2.20	14.2	11.18	0.17	7.29	11.24	2.32	0.32	0.20	300	101.0
s692_3n	tr	3	49.0	2.47	14.2	11.52	0.18	7.63	12.30	2.44	0.51	0.23	200	100.5
s692_3q		3	51.6	2.25	14.2	10.92	0.18	7.10	11.24	2.26	0.35	0.22	150	100.4
s692_3r		3	51.0	2.46	13.5	10.78	0.16	8.84	11.09	2.16	0.37	0.19	250	100.6
s692_3s		3	51.6	2.67	14.0	10.55	0.18	7.03	11.27	2.38	0.37	0.23	200	100.3
s692_3u		3	52.2	2.52	14.4	10.06	0.16	7.30	11.39	2.24	0.41	0.19	150	100.9
s692_3v	tr	3	49.4	2.94	13.6	11.31	0.16	7.16	11.83	2.13	0.42	0.26	200	99.2
s692_3w	tr	3	47.0	2.66	14.4	11.92	0.15	7.86	12.55	2.55	0.65	0.27	250	100.0
s692_3y	tr	3	49.3	2.52	14.1	11.24	0.18	7.24	11.67	2.46	0.44	0.23	150	99.4
s692_3ad	tr	3	50.4	2.31	14.3	10.51	0.17	7.46	12.39	2.24	0.40	0.25	N.A.	100.3
s692_3af	tr	3	49.0	2.47	13.4	11.85	0.18	9.11	11.30	2.30	0.53	0.26	N.A.	100.3
s692_3ah	tr	3	49.0	2.43	14.2	11.32	0.23	7.53	12.21	2.37	0.51	0.26	N.A.	100.1
s692_3ai	tr	3	49.3	2.61	14.4	11.07	0.17	7.11	12.51	2.40	0.56	0.28	N.A.	100.6
s692_3al		3	52.2	2.13	14.0	10.41	0.13	7.29	11.55	2.23	0.30	0.20	N.A.	100.3
s692_3am	tr	3	50.1	2.66	14.5	10.69	0.17	6.72	11.60	2.73	0.61	0.27	N.A.	99.9
s692_3ao	tr	3	50.9	2.39	13.9	10.84	0.16	7.68	11.84	2.20	0.32	0.22	N.A.	100.5
s692_3aq		3	52.0	2.37	14.2	10.24	0.19	7.13	10.90	2.33	0.40	0.22	N.A.	100.0
<i>Sample #4: breccia, hawaiite [7]^d</i>														
s692_4a		3	49.4	3.27	16.6	11.94	0.19	3.85	7.40	5.10	1.12	0.65	1600	99.7
s692_4b		3	49.9	3.18	16.7	11.61	0.18	3.81	7.50	4.99	1.08	0.64	1500	99.8
s692_4c		3	49.4	3.35	16.6	12.03	0.18	3.89	7.36	4.98	1.05	0.71	1650	99.7
s692_4e		3	50.6	2.93	16.1	10.77	0.19	3.43	7.37	5.05	1.26	0.70	1150	98.5
s692_4f		3	49.5	3.26	16.7	11.66	0.18	3.82	7.59	5.07	1.05	0.62	1450	99.6
s692_4ac		3	48.9	3.30	17.0	11.93	N.A.	3.71	7.58	4.87	1.09	0.47	1400	99.0
s692_4ae		3	49.3	3.21	17.1	11.49	N.A.	3.69	7.71	5.05	1.10	0.56	1300	99.4

(continued on next page)

Table 3 (continued)

	n^a	SiO ₂	TiO ₂	Al ₂ O ₃	FeO _T	MnO	MgO	CaO	Na ₂ O	K ₂ O	P ₂ O ₅	S (ppm)	Oxide total (wt.%)	
<i>Sample #5: breccia, hawaiite [12]^d</i>														
s692_5a	4	48.5	3.40	16.9	12.67	N.A.	3.86	7.27	4.81	1.12	0.51	1600	99.2	
s692_5b	3	48.3	3.46	16.9	12.75	N.A.	3.79	7.27	4.88	1.08	0.58	1500	99.1	
s692_5c	3	48.3	3.41	16.8	12.63	N.A.	3.77	7.27	5.00	1.11	0.57	1350	99.0	
s692_5d	3	48.3	3.36	17.0	12.53	N.A.	3.76	7.33	5.03	1.08	0.55	1650	99.1	
s692_5e	3	48.3	3.42	16.9	12.66	N.A.	3.74	7.27	5.04	1.11	0.54	1400	99.2	
s692_5f	3	48.4	3.40	16.8	12.60	N.A.	3.79	7.29	4.84	1.09	0.50	1450	98.9	
s692_5g	3	48.4	3.45	16.7	12.73	N.A.	3.83	7.34	4.97	1.07	0.53	1500	99.2	
s692_5h	3	48.3	3.43	16.8	12.74	N.A.	3.87	7.34	4.78	1.10	0.52	1600	99.1	
s692_5i	3	48.5	3.42	16.9	12.58	N.A.	3.89	7.27	4.81	1.08	0.56	1500	99.1	
s692_5j	3	48.5	3.39	17.0	12.59	N.A.	3.79	7.29	4.96	1.08	0.53	1500	99.3	
s692_5k	3	48.2	3.39	16.8	12.73	N.A.	3.80	7.26	5.00	1.11	0.58	1500	99.0	
s692_5l	3	48.4	3.43	16.8	12.72	N.A.	3.79	7.24	4.96	1.17	0.59	1600	99.3	
<i>Sample #7: glass sandstone, tholeiitic to transitional^c (tr) basalt [29]^d</i>														
s692_7c	3	51.9	2.45	14.0	10.40	0.17	7.01	11.52	2.19	0.36	0.23	50	100.2	
s692_7d	3	51.8	2.48	14.0	10.75	0.17	6.72	11.30	2.30	0.39	0.24	100	100.1	
s692_7e	3	52.1	2.69	13.8	11.14	0.15	6.49	10.74	2.45	0.41	0.26	150	100.2	
s692_7h	3	50.9	2.50	13.5	10.46	0.17	8.08	11.41	2.13	0.36	0.20	150	99.7	
s692_7j	3	52.0	2.58	14.3	10.72	0.17	6.91	11.26	2.32	0.39	0.24	150	100.8	
s692_7m	3	52.4	2.38	13.9	10.27	0.16	7.27	11.19	2.25	0.36	0.22	≤50	100.5	
s692_7r	3	51.9	2.40	13.9	11.06	0.15	7.10	11.37	2.25	0.35	0.23	200	100.7	
s692_7w	3	52.5	2.75	14.1	11.11	0.16	6.65	10.65	2.42	0.41	0.24	150	101.0	
s692_7x	3	52.6	2.17	14.4	10.36	0.17	7.25	11.11	2.28	0.29	0.20	150	100.9	
s692_7aa	tr	4	49.6	2.29	14.7	11.30	N.A.	6.81	12.06	2.56	0.42	0.15	1550	100.1
s692_7ab	tr	3	50.3	2.62	13.7	12.84	N.A.	6.02	11.19	2.47	0.41	0.23	1050	99.9
s692_7ac	tr	3	49.5	2.44	15.0	11.54	N.A.	6.02	11.32	2.49	0.42	0.17	1500	99.0
<i>Sample #8: glass sandstone, tholeiitic basalt [26]^d</i>														
s692_8c	3	52.2	2.49	13.9	10.78	0.16	6.97	11.40	2.22	0.36	0.21	100	100.7	
s692_8e	3	52.3	2.46	13.9	10.70	0.15	6.87	11.14	2.26	0.34	0.19	50	100.3	
s692_8f	3	52.1	2.62	14.2	10.85	0.16	6.52	11.33	2.29	0.40	0.24	150	100.8	
s692_8h	3	52.2	2.63	14.1	11.13	0.16	6.63	10.72	2.40	0.40	0.27	100	100.6	
s692_8m	3	50.4	2.23	13.9	10.99	0.16	7.53	11.81	2.19	0.28	0.18	300	99.7	
s692_8q	3	51.9	2.63	13.9	9.85	0.17	6.92	11.34	2.33	0.37	0.21	100	99.6	
s692_8s	3	52.2	2.82	13.9	10.68	0.16	7.01	10.85	2.33	0.44	0.27	100	100.7	
s692_8u	3	51.9	2.47	14.0	10.67	0.16	7.08	11.08	2.27	0.38	0.23	50	100.3	
s692_8v	3	52.5	2.35	14.2	10.65	0.17	6.96	11.31	2.26	0.31	0.22	100	100.9	
s692_8x	3	51.6	2.40	13.8	11.01	0.16	7.14	11.24	2.19	0.36	0.21	150	100.1	
<i>Sample #9: glass sandstone, tholeiitic basalt [28]^d</i>														
s692_9a	tr	5	50.6	2.30	13.6	10.41	0.15	7.52	11.44	2.14	0.40	0.23	N.A.	98.9
s692_9h	tr	3	50.6	2.80	14.0	10.38	0.16	7.51	11.76	2.14	0.39	0.23	350	100.1
s692_9j	3	51.5	2.56	14.1	10.67	0.15	7.12	11.07	2.39	0.41	0.23	200	100.2	
s692_9k	3	51.3	2.54	14.1	10.60	0.18	7.48	11.53	2.27	0.40	0.21	100	100.7	
s692_9p	3	52.2	2.44	14.4	10.63	0.17	7.04	10.86	2.40	0.38	0.20	100	100.7	
s692_9q	3	52.2	2.72	14.2	11.02	0.17	6.91	10.52	2.51	0.43	0.23	150	100.9	
s692_9r	3	51.9	2.43	14.2	10.53	0.16	7.67	11.42	2.23	0.35	0.24	100	101.1	
s692_9t	3	51.7	2.50	14.1	10.69	0.15	7.36	11.56	2.22	0.38	0.22	200	100.9	
s692_9u	3	51.2	2.21	14.3	10.98	0.17	7.52	11.61	2.28	0.30	0.22	550	100.9	
s692_9w	3	52.0	2.66	14.1	10.59	0.16	7.05	10.86	2.44	0.46	0.26	100	100.6	
<i>Sample #10: glass sandstone, tholeiitic to transitional^c (tr) basalt [26]^d</i>														
s692_10b	3	51.3	2.38	14.0	10.95	0.15	7.11	11.79	2.26	0.30	0.21	200	100.4	
s692_10e	tr	3	50.6	2.35	14.2	11.26	0.16	7.36	11.77	2.51	0.44	0.23	150	100.9
s692_10g	tr	2	50.6	2.61	14.0	11.37	0.18	6.92	11.76	2.48	0.44	0.23	150	100.6
s692_10h	tr	3	51.0	2.30	14.0	10.59	0.17	7.50	12.27	2.17	0.39	0.20	≤50	100.6
s692_10j	3	51.6	2.08	14.3	10.66	0.17	7.16	11.53	2.45	0.32	0.20	≤50	100.5	

Table 3 (continued)

	<i>n</i> ^a	SiO ₂	TiO ₂	Al ₂ O ₃	FeO _T	MnO	MgO	CaO	Na ₂ O	K ₂ O	P ₂ O ₅	S (ppm)	Oxide total (wt.%)
<i>Sample #10: glass sandstone, tholeiitic to transitional^c (tr) basalt [26]^d</i>													
s692_10n	3	51.4	2.21	14.0	10.91	0.15	7.12	11.56	2.22	0.31	0.24	150	100.1
s692_10p	3	51.5	2.26	14.0	10.95	0.13	7.46	11.24	2.38	0.36	0.25	50	100.5
s692_10s	3	52.5	2.61	13.6	10.69	0.16	6.98	10.33	2.49	0.51	0.35	100	100.2
s692_10t	tr	3	50.6	2.27	13.8	11.11	0.16	7.82	12.02	0.37	0.19	≤50	100.6
s692_10u	3	51.1	2.32	14.1	10.69	0.16	7.29	12.12	2.32	0.40	0.24	200	100.8
s692_10v	3	51.7	2.36	13.6	11.51	0.15	6.61	11.23	2.27	0.37	0.29	100	100.0
s692_10y	3	51.1	2.38	13.9	11.21	0.20	6.91	11.66	2.42	0.42	0.24	100	100.5
s692_10z	3	52.5	2.29	14.0	10.22	0.16	7.02	11.21	2.38	0.34	0.25	100	100.4
<i>Sample #11: breccia, tholeiitic to transitional^c (tr) basalt [55]^d</i>													
s692_11b	3	51.2	2.38	14.4	10.38	0.16	7.32	12.05	2.16	0.40	0.17	≤50	100.9
s692_11g	3	51.8	2.20	14.5	9.78	0.14	7.46	11.91	2.27	0.34	0.19	200	100.5
s692_11h	3	52.5	2.29	14.5	9.67	0.17	7.19	11.56	2.31	0.36	0.19	150	100.5
s692_11i	tr	7	50.6	2.43	14.6	10.34	0.16	6.77	11.40	0.44	0.25	1350	99.6
s692_11p	3	51.7	2.24	14.4	9.78	0.18	7.40	11.87	2.29	0.32	0.17	150	100.2
s692_11q	4	51.9	2.42	14.3	10.30	0.17	6.99	11.13	2.39	0.44	0.25	1150	100.3
s692_11ad	3	52.0	2.32	14.2	9.86	0.15	7.29	11.76	2.14	0.40	0.23	50	100.3
s692_11af	3	52.6	2.37	14.1	10.22	0.13	6.95	11.53	2.29	0.36	0.24	100	100.8
s692_11ag	3	51.5	2.00	14.8	9.96	0.15	7.78	11.97	2.40	0.32	0.22	≤50	101.0
s692_11an	3	52.6	2.11	14.3	9.76	0.14	7.24	11.66	2.30	0.33	0.22	100	100.6
s692_11av	3	51.9	2.30	14.1	10.18	0.16	7.14	11.59	2.26	0.33	0.23	100	100.2
s692_11bb	3	51.3	1.96	13.8	10.47	0.16	8.16	11.14	2.27	0.35	0.24	1100	99.7
s692_11bc	3	51.1	1.87	14.7	9.76	0.14	7.50	11.95	2.38	0.33	0.21	200	99.9
s692_11bi	3	52.2	2.33	14.2	9.99	0.15	6.98	11.11	2.40	0.44	0.22	950	99.8
s692_11en	3	50.4	2.42	14.7	10.24	0.16	6.46	11.24	2.48	0.48	0.25	1200	98.9
<i>Sample #12: breccia, tholeiitic basalt [43]^d</i>													
s692_12a	3	52.2	2.25	14.3	9.63	0.14	7.24	11.61	2.28	0.38	0.20	100	100.1
s692_12e	3	52.9	2.19	14.6	9.42	0.16	7.43	11.29	2.31	0.38	0.24	200	100.8
s692_12h	2	51.1	2.47	14.2	10.49	0.16	7.20	11.94	2.18	0.39	0.22	100	100.4
s692_12i	3	51.8	2.17	14.3	9.78	0.18	7.37	11.85	2.24	0.33	0.19	200	100.3
s692_12m	4	51.7	2.53	13.9	10.34	0.17	6.93	11.60	2.23	0.41	0.27	50	100.1
s692_12s	3	51.4	2.54	14.2	10.35	0.17	7.12	11.58	2.25	0.39	0.22	≤50	100.3
s692_12aj	3	52.1	2.08	14.5	9.98	0.16	7.31	11.45	2.30	0.28	0.15	100	100.4
s692_12aq	3	51.2	2.39	14.1	10.49	0.16	7.24	11.98	2.20	0.38	0.23	50	100.3
s692_12ba	4	51.4	2.10	14.0	10.52	N.A.	7.96	11.33	2.34	0.32	0.14	1000	100.2
s692_12bb	4	51.5	2.22	14.3	10.42	N.A.	7.70	11.03	2.50	0.43	0.19	850	100.4
<i>Sample #17: fossiliferous glass siltstone, tholeiitic basalt [23]^d</i>													
s692_17d	3	52.9	2.26	13.6	11.36	0.19	6.35	10.88	2.35	0.44	0.30	100	100.7
s692_17f	3	52.0	2.08	14.3	10.62	0.17	6.99	11.38	2.35	0.47	0.23	150	100.8
s692_17m	3	53.0	2.06	14.0	10.47	0.14	6.81	11.09	2.30	0.33	0.21	≤50	100.6
s692_17n	3	52.6	2.19	13.7	10.89	0.15	6.86	11.12	2.33	0.46	0.27	≤50	100.6
s692_17o	2	53.0	2.00	14.1	10.13	0.14	6.93	10.91	2.39	0.44	0.29	≤50	100.4
s692_17q	3	52.6	2.21	13.8	10.65	0.14	6.89	11.06	2.39	0.43	0.28	50	100.6
s692_17x	2	52.4	2.15	13.8	10.64	0.16	6.93	11.08	2.32	0.40	0.25	50	100.1
s692_17y	2	53.3	1.90	14.2	9.66	0.14	7.47	10.91	2.45	0.30	0.16	50	100.5
s692_17aa	3	53.1	1.75	14.2	9.99	0.15	7.25	10.85	2.40	0.33	0.21	100	100.3
s692_17ac	3	51.9	2.13	13.2	11.12	0.15	8.66	10.75	2.22	0.41	0.20	200	100.7

^a Lavas, *n* = number of spots analyzed in glass selvage; volcanoclastic glasses, *n* = number of grains analyzed (w/3 spots each) in the sample.

^b Samples from dive S690 are numbered according to the site at which they were collected; sample s690_3c was probably collected at site 7 (see text).

^c Transitional tholeiitic basalts (defined as having SiO₂ <51.0 wt.% and total alkalis >2.50 wt.%).

^d Total number of grains analyzed from the given sample. Remaining analyses available upon request from the first author.

Table 4

Laser ablation ICP-MS analyses of trace elements in glasses from dives S690 and S692 and standard BHVO-2G

	Dive S690						Dive S692							
	Tholeiitic basalt pillow lavas						Sample #3: glass sandstone, tholeiitic to transitional (tr) basalt							
	2c	3a	5b	6d	7a	8a	3d	3e (tr)	3f (tr)	3g (tr)	3h (tr)	3h1 (tr)	3i	3j
Rb	7.6	8.2	6.5	5.6	6.8	5.3	7.3	6.5	11.5	11.4	5.0	7.2	6.9	7.2
Ba	117	118	65	64	64	63	85	81	144	160	70	85	92	89
U	0.19	0.21	0.21	0.18	0.19	0.14	0.22	0.19	0.34	0.28	0.13	0.20	0.21	0.21
Th	0.96	0.92	0.50	0.53	0.45	0.49	0.69	0.74	1.42	1.35	0.69	0.71	0.80	0.78
Nb	13.0	13.2	9.6	8.8	9.0	8.8	12.2	11.2	19.7	19.4	10.5	12.3	11.9	13.2
Ta	0.92	0.94	0.57	0.54	0.53	0.61	0.82	0.73	1.30	1.30	0.74	0.80	0.80	0.92
La	13.5	13.9	8.6	8.2	7.6	8.0	11.2	10.4	17.4	17.6	10.0	11.1	11.2	12.2
Ce	26.5	27.9	24.8	22.7	23.7	20.7	26.6	25.6	38.4	35.8	21.2	26.3	26.6	29.5
Pr	4.6	4.7	3.5	3.2	3.3	3.3	3.8	4.1	5.0	5.0	3.4	3.9	4.2	4.5
Pb	0.46	0.46	0.45	0.41	0.56	0.43	0.42	0.38	0.64	0.51	0.34	0.43	0.41	0.49
Sr	331	333	251	279	287	288	305	307	417	388	268	306	317	366
Nd	21.8	21.8	16.4	15.5	15.2	16.5	17.8	19.6	21.5	23.0	16.8	18.5	20.6	21.7
Zr	174	174	114	110	101	121	117	144	129	137	115	118	142	141
Hf	4.33	4.54	2.89	2.73	2.41	3.16	3.14	3.93	3.43	3.77	3.23	3.23	3.62	3.73
Sm	6.0	6.1	4.6	4.2	4.2	4.8	4.9	5.6	5.0	5.2	4.2	4.3	5.7	5.3
Eu	1.81	1.87	1.67	1.54	1.50	1.62	1.65	1.85	1.87	1.68	1.49	1.68	1.87	1.90
Gd	6.2	6.1	4.9	4.5	4.2	5.1	4.9	5.4	4.9	5.4	4.6	4.4	5.5	5.4
Tb	1.04	1.04	0.78	0.76	0.69	0.86	0.82	0.95	0.79	0.84	0.77	0.79	0.90	0.91
Dy	6.2	6.3	4.6	4.2	4.0	5.1	4.7	5.7	4.4	4.9	4.9	4.6	5.5	5.3
Ho	1.23	1.24	0.88	0.88	0.81	1.02	0.92	1.14	0.85	0.93	0.94	0.92	1.05	1.00
Er	3.18	3.12	2.36	2.14	2.06	2.56	2.25	2.92	2.19	2.40	2.40	2.39	2.73	2.44
Tm	0.46	0.48	0.35	0.30	0.30	0.37	0.37	0.41	0.27	0.33	0.34	0.31	0.39	0.35
Y	34.3	34.7	25.5	24.6	21.8	26.7	24.6	31.3	23.0	26.0	25.5	25.4	28.7	27.0
Yb	2.66	2.67	2.02	1.78	1.82	2.21	1.96	2.29	1.71	1.90	1.92	1.91	2.22	1.89
Lu	0.41	0.41	0.30	0.28	0.25	0.33	0.29	0.35	0.24	0.28	0.29	0.27	0.34	0.28

Dive S692															
Sample #3: glass sandstone, tholeiitic to transitional (tr) basalt															
	3l	3m	3n (tr)	3q	3r	3u	3v (tr)	3w (tr)	3ao (tr)	3af (tr)	3s	3y	3ad (tr)	3ah (tr)	3ai (tr)
Rb	6.4	5.2	10.7	6.4	7.1	6.1	7.4	11.5	5.6	10.3	6.3	6.9	7.8	10.0	11.2
Ba	85	58	133	77	84	89	119	178	63	127	72	104	93	134	146
U	0.18	0.13	0.31	0.19	0.23	0.18	0.28	0.31	0.16	0.29	0.22	0.21	0.24	0.31	0.35
Th	0.68	0.53	1.10	0.61	0.69	0.83	1.15	1.60	0.56	0.98	0.81	1.09	0.76	1.11	1.48
Nb	11.3	9.0	17.7	9.9	11.8	11.9	17.8	22.5	11.1	17.4	13.1	15.6	13.1	18.1	22.2
Ta	0.79	0.61	1.19	0.67	0.82	0.90	1.27	1.46	0.78	1.15	0.94	1.15	0.87	1.18	1.41
La	11.1	7.7	15.6	9.3	9.9	11.3	14.4	20.7	9.2	15.4	11.1	14.9	12.1	15.9	19.1
Ce	26.8	18.3	34.1	23.5	26.3	24.9	32.8	41.0	22.6	35.5	26.9	27.6	30.1	33.7	40.9
Pr	4.3	3.0	4.8	3.7	3.9	4.2	5.1	5.9	3.6	5.1	4.1	4.6	4.7	4.7	5.7
Pb	0.42	0.33	0.51	0.35	0.34	0.31	0.36	0.60	0.35	0.61	0.48	0.41	0.47	0.51	0.57
Sr	323	271	387	299	295	322	345	463	308	416	295	349	355	388	415
Nd	21.6	15.0	21.3	17.5	18.8	21.0	24.4	27.0	16.9	24.0	20.2	22.0	22.2	21.7	24.2
Zr	154	107	134	123	131	154	162	171	123	151	140	165	160	141	143
Hf	4.42	2.79	3.56	3.06	3.60	4.32	4.38	4.29	3.47	4.01	3.80	4.45	3.97	3.59	3.80
Sm	6.0	4.4	5.3	4.5	4.7	5.6	5.8	6.2	4.6	5.5	5.1	6.3	6.1	5.5	6.0
Eu	2.04	1.45	1.71	1.63	1.73	1.82	1.92	2.02	1.62	1.93	1.76	1.89	2.02	1.81	1.80
Gd	6.0	4.7	5.3	5.0	5.2	6.2	6.2	6.3	4.9	5.5	5.4	6.7	6.3	5.5	6.1
Tb	1.05	0.76	0.84	0.83	0.88	1.02	1.04	0.98	0.85	0.88	0.93	1.06	1.02	0.90	0.91
Dy	6.3	4.5	4.9	4.8	5.4	6.3	6.1	5.4	5.1	5.3	5.8	6.3	6.0	5.1	5.3
Ho	1.23	0.92	0.84	0.97	0.97	1.19	1.12	1.00	0.92	0.94	1.08	1.19	1.22	0.97	0.94
Er	3.06	2.29	2.24	2.58	2.40	3.01	3.10	2.63	2.39	2.30	2.95	3.03	2.89	2.33	2.40
Tm	0.47	0.35	0.34	0.34	0.36	0.45	0.44	0.36	0.36	0.34	0.44	0.48	0.44	0.37	0.38
Y	33.4	24.8	24.5	26.1	26.3	32.0	32.7	28.1	26.4	26.3	30.5	32.6	31.4	25.5	26.5
Yb	2.57	2.00	1.86	1.98	2.11	2.47	2.35	1.88	2.10	1.86	2.40	2.50	2.49	1.91	2.04
Lu	0.39	0.29	0.27	0.33	0.31	0.38	0.34	0.28	0.31	0.23	0.36	0.36	0.37	0.29	0.29

Table 4 (continued)

Dive S692														
	Sample #3			Sample #5: breccia, hawaiiite										
	3al	3am (tr)	3aq	5a	5b	5c	5d	5e	5f	5g	5h	5i	5j	5k
Rb	4.9	7.4	7.0	22.4	23.0	20.6	21.9	21.5	19.0	17.1	16.6	17.9	21.4	24.1
Ba	53	105	90	236	234	227	227	233	226	227	226	224	234	233
U	0.15	0.22	0.22	0.71	0.71	0.63	0.69	0.63	0.59	0.52	0.52	0.56	0.62	0.70
Th	0.46	0.97	0.64	2.17	2.22	2.17	2.10	2.11	2.17	2.34	2.51	2.39	2.21	1.97
Nb	8.0	15.3	11.7	42.9	41.7	41.6	41.8	42.3	42.7	41.5	41.0	41.8	43.9	43.1
Ta	0.56	1.05	0.75	2.64	2.56	2.63	2.65	2.61	2.84	2.86	2.96	2.90	2.85	2.71
La	7.7	13.6	11.1	30.4	30.2	29.8	29.6	29.8	31.9	33.8	34.4	33.2	31.4	30.2
Ce	19.5	28.3	27.9	72.6	73.8	68.9	70.0	69.2	68.9	68.3	67.9	70.2	73.8	75.0
Pr	3.1	4.2	4.4	10.3	10.4	10.0	9.9	10.4	10.3	10.6	10.5	10.5	10.4	10.2
Pb	0.32	0.46	0.48	1.58	1.22	1.02	1.11	1.07	0.97	0.82	0.82	1.00	1.09	1.18
Sr	264	336	331	779	776	764	772	777	757	780	783	755	779	767
Nd	15.0	20.6	21.1	46.7	48.7	46.1	45.6	46.8	47.3	49.3	50.3	49.2	47.6	46.0
Zr	108	142	153	329	328	331	324	346	369	402	409	380	355	342
Hf	2.94	3.63	4.02	7.40	7.66	7.57	7.93	7.81	8.63	9.50	10.19	9.39	8.11	7.75
Sm	4.3	4.7	5.5	11.0	10.8	10.2	10.4	10.9	11.3	12.4	12.3	12.4	11.6	11.3
Eu	1.42	1.73	1.92	3.52	3.66	3.60	3.55	3.54	3.71	3.80	3.79	3.76	3.73	3.55
Gd	4.3	5.1	6.1	11.1	11.1	10.7	11.1	11.1	11.1	11.8	11.7	11.6	10.5	10.3
Tb	0.77	0.85	0.98	1.63	1.68	1.61	1.61	1.66	1.68	1.84	1.84	1.81	1.70	1.52
Dy	4.5	5.0	6.3	10.2	9.7	9.4	9.7	9.7	10.0	10.9	11.0	10.3	9.3	8.9
Ho	0.86	0.97	1.20	1.71	1.68	1.66	1.67	1.70	1.94	2.12	2.16	2.05	1.76	1.71
Er	2.39	2.54	2.98	4.29	4.47	4.60	4.61	4.58	4.86	5.69	5.41	5.24	4.57	4.39
Tm	0.37	0.38	0.43	0.61	0.62	0.62	0.61	0.63	0.68	0.78	0.79	0.73	0.68	0.61
Y	25.1	28.1	31.6	45.1	45.2	46.0	44.8	45.9	51.6	57.8	58.4	52.8	48.7	45.0
Yb	1.96	2.03	2.36	3.62	3.62	3.56	3.72	3.73	3.91	4.41	4.42	4.23	3.71	3.41
Lu	0.28	0.32	0.36	0.54	0.55	0.56	0.53	0.56	0.59	0.69	0.66	0.67	0.56	0.52

Dive S692														
	Sample #7: glass sandstone, tholeiitic to transitional (tr) basalt									Sample #10: glass sandstone				
	7e	7h	7j	7m	7r	7w	7x	7aa (tr)	7ab (tr)	7ac (tr)	10b	10e (tr)	10g (tr)	10h (tr)
Rb	7.4	7.0	7.2	6.7	6.5	5.8	4.8	6.7	6.8	7.4	6.6	9.9	12.6	11.2
Ba	84	93	78	86	79	77	65	84	88	88	66	112	104	92
U	0.24	0.24	0.24	0.25	0.19	0.23	0.17	0.18	0.24	0.26	0.18	0.30	0.38	0.30
Th	0.76	0.76	0.72	0.87	0.68	0.97	0.64	0.83	1.04	0.90	0.53	0.89	0.73	0.66
Nb	12.7	12.7	11.1	12.3	10.7	11.9	8.8	11.4	14.1	13.0	11.0	16.3	15.2	13.3
Ta	0.85	0.87	0.79	0.80	0.75	0.91	0.67	0.93	1.10	0.89	0.73	1.00	0.87	0.74
La	11.5	11.2	10.5	11.4	10.2	12.4	8.9	11.2	13.4	12.1	8.4	12.7	11.5	9.7
Ce	29.2	29.4	28.0	29.4	26.6	28.3	23.1	25.0	29.6	29.6	22.0	31.7	37.7	31.1
Pr	4.4	4.2	4.2	4.3	3.9	4.4	3.5	3.9	4.6	4.3	3.2	4.3	4.4	3.8
Pb	0.45	0.42	0.41	0.40	0.39	0.34	0.33	0.40	0.42	0.46	0.45	0.70	1.20	0.79
Sr	304	307	313	289	298	278	278	335	308	331	274	350	356	327
Nd	20.8	19.5	19.8	20.6	19.1	22.1	16.6	18.8	22.7	19.9	15.6	19.1	18.5	15.6
Zr	157	134	145	140	131	181	123	138	168	134	106	120	94	94
Hf	3.87	3.41	3.63	3.58	3.65	5.03	3.23	4.01	4.55	3.75	2.60	2.96	2.51	2.16
Sm	5.7	5.2	5.2	4.9	5.1	5.7	4.5	4.9	5.9	5.2	4.7	4.9	4.4	4.3
Eu	1.86	1.65	1.67	1.59	1.68	1.83	1.53	1.64	1.79	1.55	1.55	1.65	1.60	1.43
Gd	6.1	5.1	5.3	4.9	4.9	5.6	4.3	4.8	5.8	4.5	4.5	5.1	4.3	3.8
Tb	0.96	0.79	0.88	0.83	0.80	1.01	0.79	0.85	1.00	0.76	0.76	0.75	0.66	0.60
Dy	5.8	4.9	5.1	4.9	4.9	6.3	5.1	5.2	6.0	4.6	4.5	4.4	4.0	3.7
Ho	1.17	1.00	1.02	1.06	1.02	1.38	1.11	1.10	1.27	0.97	0.89	0.82	0.72	0.64
Er	3.18	2.77	2.71	2.82	2.53	3.71	2.68	2.81	3.19	2.50	2.22	2.16	1.81	1.70
Tm	0.44	0.37	0.39	0.39	0.39	0.52	0.40	0.41	0.46	0.36	0.32	0.30	0.24	0.24
Y	32.7	27.7	28.9	28.9	27.4	38.6	29.1	28.9	35.8	27.1	23.2	22.8	19.6	18.8
Yb	2.86	2.38	2.44	2.46	2.46	3.07	2.33	2.48	2.95	2.23	1.84	1.77	1.49	1.39
Lu	0.38	0.31	0.33	0.33	0.35	0.46	0.36	0.35	0.42	0.33	0.27	0.27	0.22	0.20

(continued on next page)

Table 4 (continued)

	Dive S692									Standard	
	Sample #10: glass sandstone, tholeiitic to transitional (tr) basalt									BHVO-2G	
	10j	10n	10p	10s	10t (tr)	10u	10v	10y	10z	AVG ^a	1σ
Rb	6.6	6.0	7.8	11.8	6.3	9.5	7.9	9.8	7.8	9.2	(0.5)
Ba	70	58	73	113	79	94	74	92	71	127	(3)
U	0.21	0.19	0.22	0.35	0.19	0.25	0.21	0.27	0.22	0.42	(0.04)
Th	0.52	0.47	0.53	0.82	0.67	0.79	0.57	0.64	0.53	1.20	(0.12)
Nb	10.7	9.3	11.3	14.8	12.0	15.4	12.0	14.4	11.3	18.4	(0.5)
Ta	0.65	0.55	0.69	0.89	0.79	0.91	0.75	0.84	0.70	1.19	(0.06)
La	8.7	8.2	9.2	13.2	10.3	11.6	9.2	10.9	8.6	15.5	(0.7)
Ce	24.4	22.3	26.0	37.6	25.3	30.7	25.8	30.5	25.6	36.8	(1.3)
Pr	3.4	3.4	3.6	5.2	3.8	4.2	3.7	4.1	3.4	5.5	(0.2)
Pb	0.56	0.52	0.55	0.81	0.48	0.82	0.56	0.70	0.60	1.57	(0.11)
Sr	290	288	300	309	315	324	291	338	301	394	(8)
Nd	15.8	15.7	16.5	23.7	17.5	18.4	17.6	18.1	16.1	24.9	(0.6)
Zr	99	101	105	158	118	113	109	115	102	165	(5)
Hf	2.45	2.50	2.58	3.75	3.03	2.83	2.92	2.93	2.87	4.16	(0.33)
Sm	4.2	4.0	4.4	5.9	4.2	4.5	4.5	4.7	4.2	6.0	(0.3)
Eu	1.42	1.50	1.58	2.04	1.65	1.71	1.67	1.77	1.70	2.00	(0.08)
Gd	3.8	4.0	4.3	5.7	4.8	4.8	4.7	5.1	4.6	6.0	(0.2)
Tb	0.64	0.68	0.67	0.93	0.77	0.73	0.75	0.72	0.71	0.91	(0.05)
Dy	4.0	4.1	4.1	5.7	4.5	4.3	4.6	4.3	4.1	5.3	(0.2)
Ho	0.75	0.79	0.79	1.05	0.84	0.81	0.83	0.77	0.78	0.97	(0.04)
Er	2.03	2.02	2.01	2.75	2.20	2.08	2.33	1.99	2.09	2.47	(0.14)
Tm	0.27	0.30	0.30	0.41	0.33	0.30	0.30	0.29	0.31	0.35	(0.02)
Y	20.8	22.2	21.6	29.5	24.2	23.2	23.4	22.4	22.6	26.8	(1.0)
Yb	1.66	1.75	1.72	2.29	1.86	1.79	1.96	1.90	1.91	1.94	(0.11)
Lu	0.25	0.26	0.23	0.33	0.27	0.26	0.28	0.25	0.25	0.29	(0.03)

Each reported sample value is the average of ≥ 3 spots. All values are in ppm.

^a Average of 46 analyses.

MgO concentration, with no corresponding enrichment of Al₂O₃.

4.3.3. Sulfur contents

The sulfur contents of glasses from dive S690 vary widely. Lavas collected from 3002 to 2782 mbsl have S contents 1400–1150 ppm, lavas from 2518 mbsl have 200–250 ppm, and lavas from 2445 to 2104 mbsl have 700–800 ppm S. The groupings in S content are mirrored by major and minor element distributions (note groupings in K₂O, P₂O₅, etc., Table 3) and probably reflect sampling of three separate flow units. These results contrast with those from the recent *Kaiko* dives on the slump, where lavas have tightly clustered, intermediate S contents (Lipman and Coombs, 2006–this issue). The K218 and K219 lavas were collected are 3900–3000 and 3500–2700 mbsl respectively.

Hawaiite glasses from dive S692 (#4 and #5) contain 1150–1650 ppm S (Table 2; Fig. 2C). The majority of basalt glasses (97% of tholeiitic and 78% of transitional) collected during dive S692 are S-poor. However, several samples contain S-rich fragments. These comprise tholeiitic and transitional basalt in approximately

equal proportions (Fig. 2C). High-S grains are easily distinguished by their darker color (Fig. 4D), so we are reasonably certain that all of the S-rich grains (<1% by number) in our thin sections were analyzed. The S contents of these samples are a striking contrast to the major element groupings. Whereas samples #7–12 and #17 are coincident on variation diagrams and a plot of total alkalis versus silica (TAS diagram), only the glass grains in #8, #10, and #17 are internally uniform in S content, and all with very low values. Samples #7, #11, and #12 contain shards that are at or near the MORB sulfide saturation curve (Wallace and Carmichael, 1992) at eruption temperatures (1115–1260 °C).

4.4. Glass ICP-MS analysis and trace element concentrations

Trace element concentrations of 60 glass shards and pillow selvages from both dives (Table 4), many of the same shards analyzed by EMP, were measured using laser ablation ICP-MS at Shimane University, Japan, using methods described in Coombs et al. (2004b). Because ablation fractionation of elements is matrix

dependent, the USGS reference material BHVO-2G was used as a standard. It is a fused form of BHVO-2, a powdered sample of basaltic lava erupted in 1919 from Kīlauea (Wilson and Taggart, 2000); an official open file report for this standard is not yet available (Stephen Wilson, pers. comm.). Reproducibility was tested by replicate analysis of the standard (Table 4). Typical reproducibility is within 5% for most of the elements and slightly poorer results for Tb, Lu, Hf, Th, Pb, and U (<11%). These values represent the analytical uncertainty associated with analysis of unknowns. The analytical errors, assessed as the median 1σ values for replicate analyses, are <7% relative for all elements analyzed, indicating that the glasses are homogeneous to within analytical precision.

Concentrations of highly incompatible elements form simple, positively sloping arrays in variation diagrams (Fig. 8). The S690 and S692 tholeiites and

transitional basalts form a coherent trend that is coincident with previously published Hualālai tholeiite compositions (Gurriet, 1988; Norman et al., 2002); post-shield Hualālai alkalic basalts are scattered. All of the new analyses form similar primitive mantle (PM)-normalized trace element abundance patterns (Fig. 9). Transitional basalts and tholeiites are coincident in both the range of values and slope of moderate to heavy REE, and both series plateau at Zr and Hf (Fig. 9A and Table 4). For elements more incompatible than Nd, transitional basalts fan out from the tholeiite to encompass more enriched concentrations of LREE, HFSE and LILE, with patterns that are subparallel to the tholeiites. The abundance pattern of S692 hawaiite (sample #5, Fig. 9B) is nearly perfectly parallel to that of enriched transitional basalt, elevated by a factor of 1.9; the exceptions include slightly increased Zr, Hf, Nb, and Ta concentrations and depressed Ba contents in the hawaiite (see also Fig. 8).

Although Pb is prone to volatilization during ablation, acceptable analyses of the standard BHVO-2G suggest that matrix-dependent fractionation effects during analysis were minimal. All S690 and S692 samples have Pb concentrations that are low relative to other similarly incompatible elements (Table 4), and form negative Pb anomalies on PM-normalized diagrams (Hofmann, 1997); the Pb values are omitted from Fig. 9 for the sake of clarity. One possibility for anomalously low Pb that is consistent with high Ce/Pb values in these samples (46–90; Table 4) compared to ~30 for oceanic basalt (Hofmann, 1997; Huang and Frey, 2003) is that Pb volatilized during magmatic degassing.

5. Volcanic affinities

Samples #1 and #2 are inferred to have originated from Mauna Loa and to have been transported to their present location in the 'Ālika 2 landslide; we do not consider them further in the following discussion of the North Kona slump or development of Hualālai volcano. The truncated and draping tholeiitic lavas sampled during dive S690 are clearly products of Hualālai volcano's magmatic system, based on their location along the volcano's northwest rift zone and their compositions, similar to others dredged from the rift (Moore and Clague, 1992). Origins of the S692 sliver materials are less certain, and trace element data may allow evaluation of our inference that the materials in the elongate sliver derive from Hualālai. For example, the high field strength element ratio Zr/Nb varies systematically among mantle sources beneath some Ha-

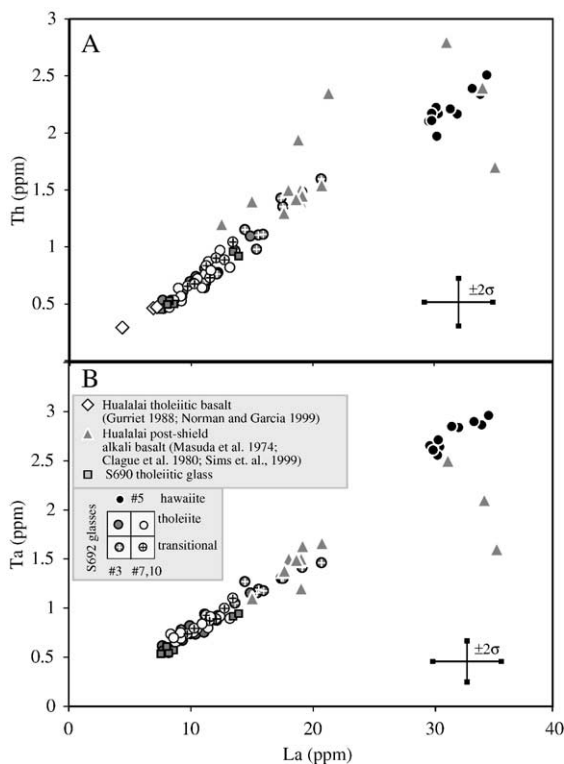


Fig. 8. Variation of highly incompatible elements that are resistant to chemical alteration. La–Th (A) and La–Ta (B) among Hualālai tholeiitic basalt (Gurriet, 1988; Norman and Garcia, 1999), post-shield alkalic basalt (Masuda et al., 1974; Clague et al., 1980; Sims et al., 1999), S690 tholeiite and S692 tholeiite and transitional basalt (this study) form coherent linear trends that project to near the origin. Dive S692 hawaiite analyses are co-linear with other samples in La–Th, but lie slightly above the La–Ta trend shared by other Hualālai samples. Post-shield alkalic samples are heterogeneous in both La–Th and La–Ta.

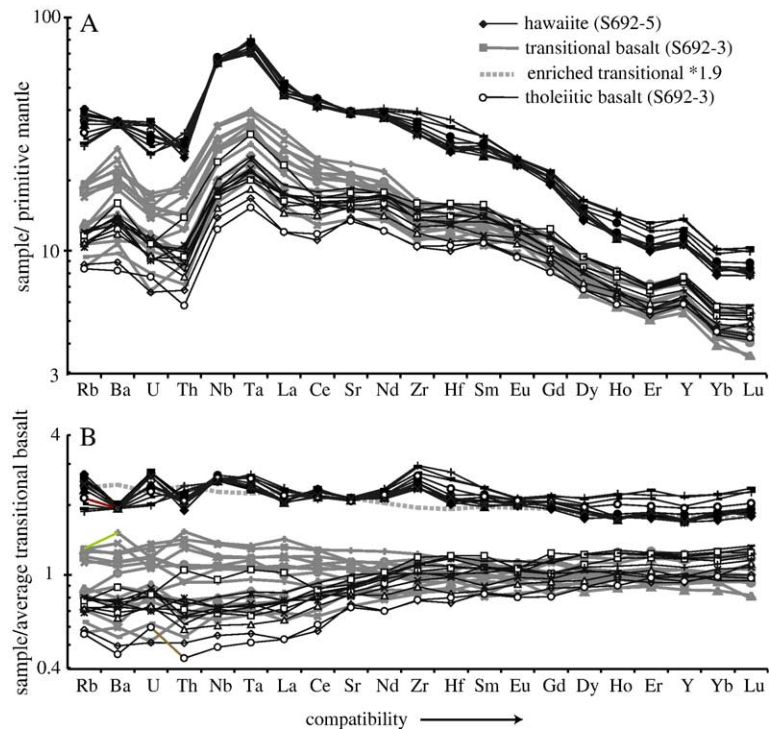


Fig. 9. Concentrations of trace elements relative to abundances in primitive mantle (McDonough and Sun, 1995) and the average S692 transitional basalt glass. Element compatibilities in oceanic basalts generally increase from left to right (after Hofmann, 1988). (A) The restricted range of the hawaiite values suggests that the glass fragments analyzed are pieces of a single, autobrecciated pillow lava. The variation in glass fragments within glass sandstone sample #3 encompasses the ranges of all the tholeiite and transitional basalt glasses in samples #7 and #10, which have been omitted for clarity. The S690 glassy lava selvages (not shown) are virtually identical to the S692-3 tholeiitic basaltic glasses. (B) Elements are normalized by the concentrations in average transitional basalt. The hawaiite pattern is parallel to the transitional basalts, whereas the tholeiites are depleted in the more incompatible elements. Short-dashed line shows the average of five most enriched transitional basalts multiplied by 1.9 for comparison with hawaiite.

waiian volcanoes (Yang et al., 1994; Norman and Garcia, 1999; Rhodes and Vollinger, 2004). Glasses from the S690 lava samples have Zr/Nb ratios that range from 11.2 to 13.3. Previously described Hualālai tholeiites are similar, with Zr/Nb values from 10.4 to 14.0 (Gurriet, 1988; Norman and Garcia, 1999). However, the ratio in transitional and tholeiitic glass fragments of S692 sandstones, which are comparatively unconstrained with respect to volcanic source, range from 6.17 to 15.3. This span surpasses known Hualālai values and those of Mauna Kea tholeiites, which cluster at 9–14 (Frey et al., 1990, 1991; Hofmann and Jochum, 1996; Wolfe et al., 1997; Huang and Frey, 2003). Apparently, Zr/Nb cannot be used to distinguish Hualālai from Mauna Kea magmas, although they both extend significantly below the characteristic Mauna Loa range in Zr/Nb of 13–16 (Kurz et al., 1995; Rhodes and Hart, 1995; Cohen et al., 1996; Hofmann and Jochum, 1996; Rhodes, 1996). The S692 hawaiite samples have Zr/Nb ratios that are lower still, from 7.66 to 9.97.

A monogenetic provenance for *all* volcanoclastic particles in the sliver is unlikely, and heterogeneity in the trace element ratios of S692 glass sandstones (samples #3, #7, #10) suggests that sources besides Hualālai may be represented in them. Although it is not possible to quantify contributions from Mauna Kea, Māhukona, or other candidates in the absence of isotopic data, similarities in transitional basalt compositions and proximity of shield-stage Māhukona, in particular, suggest it could be a source of fine-grained volcanoclastics in the sliver. Unfortunately, trace element data for Māhukona lavas are not available. Coarse breccias located above sample #10 (Fig. 2) are more likely to be proximally deposited than finer grained sandstones, have major and volatile-element trends that overlap the sandstones (including S-rich and S-poor tholeiites and transitional basalt fragments; Table 3), and are less equivocally derived from Hualālai. The position of the sampling site normal to, and immediately downslope from, the North Kona slump is probably the strongest evidence that Hualālai is the

dominant, if not exclusive, source of the volcaniclastics collected during dive S692.

6. Mantle melting and magmatic processes at Hualālai Volcano

Hualālai Volcano is presently in the post-shield alkalic stage and the vast majority of its subaerial surface is blanketed by alkalic basalt (the notable exception being a 100 ka trachyte flow and pumice cone; Moore et al., 1987). Difficulty accessing buried tholeiite is one reason that compositional data from the volumetrically dominant stage in the volcano's edifice are scarce. Hualālai shield stage is presently documented by samples recovered during water well drilling, shallow submarine dredges, and dives (Clague, 1982; Moore and Clague, 1987, 1992; Moore et al., 1987; Norman and García, 1999). The new analyses of S692 and S690 dive samples significantly augment the database of Hualālai's tholeiitic magmatic stage. Furthermore, the hawaiites collected at the lowest stratigraphic level (samples #4 and #5) appear to represent a period of alkalic volcanism, either from the pre-shield or early shield stage of volcano growth. Their high S contents indicate deep submarine eruption, and they share lithologic and geochemical features with Hilina glasses erupted during Kīlauea's pre-shield stage (Sisson et al., 2002). However, the absence of unfractionated alkalic magmas and the abundance of transitional and tholeiitic compositions in the immediately overlying strata (notwithstanding the possibility of a cryptic unconformity) suggest that the hawaiites were erupted early in the volcano's shield building stage. If this basal breccia unit indeed contains material from Hualālai juvenile (i.e., petrologically formative) development, then Hualālai becomes the third volcano exhibiting evidence of early alkalic magmatism, after Lō'ihī and Kīlauea. It also becomes the first volcano for which samples of both early and post-shield alkalic magmas have been recovered. Proceeding from the geological evidence described above, we infer that the majority of glass sands in the elongate ridge derive from Hualālai, and qualitatively consider the implications of the S690 and S692 geochemical data sets for time-varying magma genesis beneath Hualālai Volcano.

Major element-based magmatic affinities within the Hualālai data set are discriminated somewhat by HFSE and LREE concentrations. For example, the Zr/Nb ratio decreases and La/Sm ratio increases with increasing alkalinity. The Hualālai data progress from heterogeneous and highly LREE-enriched magmas in the alkalic to transitional magmas toward homogeneous, less-enriched magmas in the tholeiitic shield stage (Fig.

9), followed by a return to highly LREE-enriched signatures, e.g., La/Sm=2.8–3.9, during the post-shield stage (Clague et al., 1980; Anonymous, 1981; Sobolev et al., 1990; Sims et al., 1999). This sequence is consistent with generally lower extents of partial melting during the juvenile and post-shield stages and greater extents of partial melting during the shield stage, although differences in the trace element compositions and mineralogy of parent mantle may also be important.

The linear La/Yb–Ce trend among the S692 tholeiites (Fig. 10A) is consistent with a relationship either by varying extents of partial melting of a similar mantle source, or mixing of two magmas produced from compositionally different sources. Although isotopic data are needed to evaluate magma mixing, the nature of the relationship by varying extents of melting is fully consistent with the generally accepted model for melting in the Hawaiian plume (Chen and Frey, 1983; Frey and Clague, 1983).

6.1. Origin of hawaiite

The hawaiite (samples #4 and #5) is a highly evolved product of crystal fractionation, as indicated by low Mg# (34–37). The major and trace element compositions of these glasses provide clues about the depth of their formation and the magmatic affinity of parental melts. The relationship between Mg# and CaO/Al₂O₃ (Fig. 11) strongly suggests that clinopyroxene was an important fractionating phase in the formation of the hawaiites. One possibility is that the hawaiites were formed by fractional crystallization of clinopyroxene from an alkalic basalt melt (Macdonald, 1968). Phase equilibrium experiments demonstrate that with increasing pressure, the clinopyroxene phase volume expands at the expense of olivine (Kushiro, 1969; Mahood and Baker, 1986; Sack et al., 1987), although the position of the pseudo-cotectic is poorly constrained below 8 kb. For example, post-shield hawaiitic Mauna Kea lavas were apparently derived from precursor alkalic basalt by extensive fractionation of clinopyroxene and Fe–Ti oxides (West et al., 1988; Frey et al., 1990), at a depth significantly greater than the shield stage magma chamber levels (3–7 km), and possibly nearer 20 km (Clague et al., 1987; Frey et al., 1990). The only alkalic magmas erupted from Hualālai that are available for consideration as potential petrogenetic relatives are the post-shield basalts that cap the edifice. However, primitive basalts with incompatible trace element concentrations resembling the post-shield lavas could not give rise to the hawaiites by crystal fractionation. Yb is less incompatible than La in clinopyroxene as well as

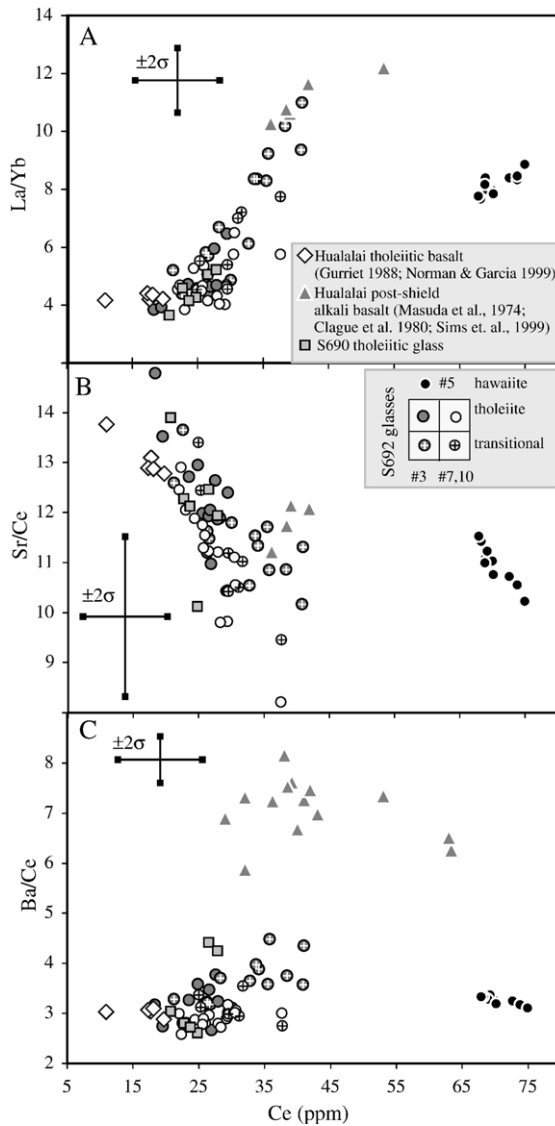


Fig. 10. Process discrimination diagrams for S690, S692 glasses and published Hualālai magmas. The concentration of Ce, highly incompatible in minerals forming in basalt, is plotted versus ratios of highly and moderately incompatible elements: La/Yb (A), Sr/Ce (B), and Ba/Ce (C). Positively sloped trends among S692 tholeiites and transitional basalts in (A) may be caused by variable extents of batch melting (with progressively increasing melt fraction toward the lower left end of the trend) or magma mixing. The transitional basalts have ratios consistent with a relationship to hawaiites by fractional crystallization, while the horizontal trend relating these melts in (B) indicates that plagioclase cannot have been in the fractionating assemblage. Post-shield magmas have elevated Ba/Ce compared to older known Hualālai tholeiites and the glasses analyzed in this study (C).

olivine (Fujimaki et al., 1984). Crystallization of either or both of these minerals would cause the La/Yb ratio of the melt to increase, yet the S692 hawaiites have

lower La/Yb ratio than the post-shield alkalic basalts (Fig. 10A).

A subset of the S692 transitional basalts have trace element proportions that are capable of producing the hawaiite values by crystal fractionation (Figs. 9 and 10A, B). Moreover, production of alkalic magmas from tholeiitic basalt is a plausible consequence of clinopyroxene fractionation, again facilitated at moderately high pressure by shifting phase boundaries (e.g., O'Hara, 1968). Fractionation of clinopyroxene, rich in Si compared to olivine, drives the liquid line of descent of residual liquids toward alkali enrichment and Si-depletion, and could produce the observed major element variation trends of the S692 hawaiites. A similar line of evidence is reported for juvenile hawaiite at Kīlauea for its derivation from transitional basalt (Sisson et al., 2002), and high-pressure clinopyroxene fractionation is also suggested to explain co-erupted magmas of tholeiitic and alkalic affinities at Galapagos volcanoes (Naumann and Geist, 1999).

If the hawaiite parent melts are transitional basalts, then plagioclase cannot have been an important fractionating phase in their formation. Plagioclase crystallization would decrease the Sr/Ce ratio of derivative

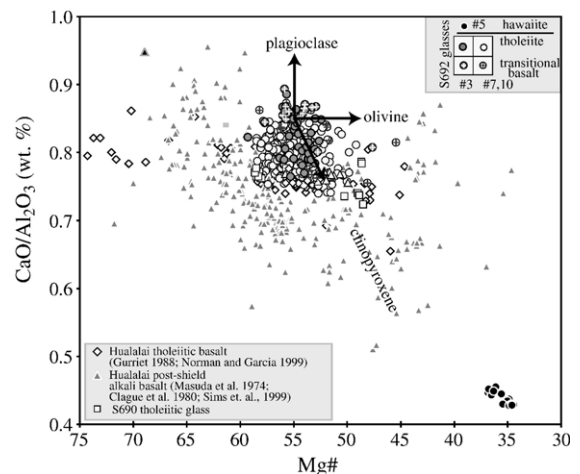


Fig. 11. Mg# versus CaO/Al₂O₃ variation diagram showing samples collected on dive S692 (Table 2) and post-shield Hualālai alkalic glasses, subdivided as subaerial basalts (Clague et al., 1980; Moore and Clague, 1987; Moore et al., 1987; Kauhikaua et al., 2002), and submarine basalts (Moore and Clague, 1987). Mg# is defined as molecular Mg/(Mg+Fe)*100. The olivine, clinopyroxene, and plagioclase mineral control lines have their origin at a Hawaiian basanite composition simply for reference (Clague and Frey, 1982). This does not imply that this basanite is parental to the alkalic magmas of Hualālai. The slope of the clinopyroxene control line is calculated for pyroxene and olivine crystallizing from MORB parent melt in the proportions ~3:1 (Stakes et al., 1984), but any clinopyroxene composition will drive liquid into the lower right quadrant of the diagram.

liquids, yet the hawaiite Sr/Ce values are not significantly lower than those of the transitional basalts (Fig. 10B). Early fractionation of plagioclase also would have driven up CaO/Al₂O₃ in the liquid. Thus although plagioclase is a dominant phenocryst in the hawaiite samples, it evidently appeared late in the crystallization sequence.

The high CaO/Al₂O₃ signature of the S692 transitional basalts (Fig. 11) may be a common feature originating in the melting regime beneath incipient Hawaiian volcanoes. Other examples include transitional basalts from Kīlauea's Hilina bench that are richer in CaO than tholeiites for a given MgO and are interpreted to have erupted early in Kīlauea's shield stage (Sisson et al., 2002), and transitional glasses collected below a submarine slope break at Māhukona volcano that are also rich in CaO for a given MgO (Clague and Moore, 1991). Lō'ihi glasses have higher CaO contents than similarly evolved basalts from shield stage volcanoes (García et al., 1995). Thus, high CaO/Al₂O₃ appears characteristic of transitional basalts. This correlation may reflect relatively small extents of partial melting, which are consistent with slightly elevated incompatible element concentrations of transitional basalts compared to tholeiites (e.g., Ti and Na; Fig. 6, and LILE-HFSE-LREE; Fig. 9). A constraint on the depth of transitional basalt formation is provided by experimentally determined pressure–melt fraction–CaO/Al₂O₃ relationships, compiled by Sisson et al. (2002; Fig. 9). The high CaO/Al₂O₃ ratio in transitional basalts (0.75–0.90) suggests that segregation of a parent melt occurred within the garnet stability field, at a minimum pressure of 35 kb. At this pressure, the CaO/Al₂O₃ ratio of partial melts is approximately 0.85 for extents of melting ≤15 wt.%.

6.2. Early shield versus post-shield alkalic magmas from Hualālai

Post-shield alkali basalts contain elevated Ba/Ce compared to magmas from previous stages, including the hawaiites (Fig. 10C). The post-shield rocks also have higher K₂O/P₂O₅ (2.75 ± 0.57) and lower Zr/Rb ratios (4.21 ± 0.50) than the hawaiite (1.75 ± 0.28 and 18.0 ± 4.8, respectively). Elevated concentrations of Ba, K, and Rb in the post-shield alkalic magmas relative to Ce, P, and Zr (Figs. 9 and 10) suggest a role for phlogopite in magma genesis, into which these otherwise highly incompatible elements are incorporated. If phlogopite were residual to mantle melting, the concentrations of these elements would be depleted in the melt relative to other incompatible elements, such as Th

(Class and Goldstein, 1997). The opposite relationship appears in the sparse data available: Ba/Th in post-shield basalts (202–206) (Sims et al., 1995) is greater than the ranges of hawaiite (90–120) and the shield-stage tholeiitic and transitional basalts (80–144). Rb/Th ratios in post-shield basalt (12–16) are greater than those of hawaiite (6–12), and similar to shield basalts (6–17). Residual phlogopite is not consistent with these data. Alternatively, melts derived from a primitive parent could contain high Ba, K, and Rb if melting just exhausted phlogopite in the mantle source, liberating these elements into the melt phase. Extents of melting much beyond the point of phlogopite exhaustion would progressively dilute the concentrations of these elements in the melt, and the signature would be erased. However, the possibility of phlogopite saturation in the parent melts is not likely given modest absolute K₂O contents (<1 wt.%) in post-shield alkalic lavas (Clague et al., 1980; Sims et al., 1999). A third possibility is that melts derived from phlogopite-bearing cumulates, formed at the point of phlogopite exhaustion, contributed to formation of the basalt. Several juvenile alkalic samples from the outer scarp of Kīlauea's Hilina bench appear to have formed in this manner (Sisson et al., 2002). Finally, the absence of a phlogopite signature in the juvenile and main shield stage magmas from Hualālai may result from either melting of a phlogopite-free source, or simply melting beyond the point of phlogopite exhaustion.

7. Growth of Hualālai and 'a sulfur dilemma'

Dissolved sulfur contents of volcanic glasses can provide useful information about eruption environment: subaerially erupted lavas lose most of their sulfur during degassing, resulting in S < ~350 ppm, whereas submarine-erupted lavas retain S due to hydrostatic pressure (e.g., Moore and Fabbri, 1971). The S content of submarine-erupted basalts can range from the presumed original magmatic S content (1000–1400 ppm; Wallace and Carmichael, 1992) to substantially lower values, the latter due to pre-eruptive processes such as mixing between degassed and undegassed lavas (e.g., Dixon et al., 1991) or eruption in shallow water (<1000 m).

The S contents of the S692 glasses, unlike the glass rinds of in-place pillow rinds from dives K218 and K219 (Lipman and Coombs, 2006-this issue) and S692, appear to be either low- or high-sulfur, with very few intermediate values (Fig. 2C). The S contents show that the hawaiites and a few of the tholeiitic and transitional glasses erupted in deep water with little loss

of magmatic sulfur. In contrast, the majority of tholeiitic and transitional glasses experienced substantial degassing, as shown by S contents of less than 350 ppm. If high CaO contents, correlated with transitional major-element compositions and variable La/Sm, typify early shield volcanism, and Hualālai at that time was a bump on the submarine flank of Mauna Kea, how did the vast majority of tholeiitic and transitional magmas observed in dive S692 experience degassing at low pressure? Perhaps Hualālai emerged above sea level relatively early in its shield stage so that compositionally transitional magmas were erupted subaerially or processed in shallow conduits. Credence to this hypothesis comes from comparison of Hualālai (and its substrate Mauna Kea) to Kīlauea (Mauna Loa). Perched on the relatively shallow flank of Mauna Loa, juvenile Kīlauea rose above the sea surface during its alkalic pre-shield stage (Coombs et al., 2006-this issue). Similarly, Hualālai may have achieved subaerial exposure relatively early in its magmatic history compared to Hawaiian volcanoes that grow from the sea floor.

A related issue is the presence of relatively young (i.e., main-to-late shield stage), tholeiitic lavas with intermediate volatile contents that drape the North Kona slump deposit (sampled in dives K218, K219; Lipman and Coombs, 2006-this issue), and the head-wall region of the slump (sampled during dive S690). Eruption of partially degassed lavas draping the mid-slope bench apparently postdates the eruption of subaerially degassed volcanoclastic glasses found in the sliver. This represents an inversion of the conventional sequence of increasingly degassed magmas appearing over time as a shallow conduit system develops with volcano growth above sea level. One possible explanation is that undegassed magmas passed through the northwest rift zone or the summit magma reservoir and mixed with degassed magmas to produce the erupted magmas having intermediate volatile contents (Dixon et al., 1991; Davis et al., 2003). This seems plausible for the S692 lavas sampled below the northwest rift zone, but is problematic for the *Kaiko*-sampled lavas, especially those of dive K219, which is not downslope from a rift zone. Another possible explanation is that lavas collected during K219 erupted from flank vents of Mauna Loa rather than Hualālai, as this site is near the presumed submarine contact between the two volcanoes. Alternatively, radial vents may be more common at Hualālai than is commonly appreciated. Several non-rift zone vents have been mapped and described on Mauna Loa's subaerial flanks (Stearns and Macdonald, 1946; Lipman, 1980; Wolfe and Morris, 1996). Submarine radial vents have also been dis-

covered on Mauna Loa's west flank (Davis et al., 2003; Wanless et al., 2006-this issue), although such vents appear to be relatively rare on the unbuttressed (spreading) flanks of Hawaiian volcanoes, as discussed by Lipman and Coombs (2006-this issue). On the other hand, the sparse sampling of submarine flanks and subdued morphology for flank vents could cause their prevalence to be underestimated. A final option is that the draping lavas erupted before the volcano emerged above sea level, and that they retain the volatile signature of shallow submarine eruption with partial resorption during emplacement (Lipman and Coombs, 2006-this issue). However, this interpretation precludes the possibility that any of the subaerially degassed volcanoclastics in the S692 sliver derive from Hualālai, as we infer from the physiographic and geochemical observations described above.

8. Landslide models

The regional North Kona bathymetry implies that a significant portion of Hualālai submarine flank collapsed to create the North Kona slump. Unfortunately, direct examination of slump materials was not possible at the K218 and K219 dive sites, due to draping of the slump by younger tholeiite pillow lavas (Lipman and Coombs, 2006-this issue). However, lithologies within the outlying elongate sliver indicate that this feature may have been a fragment of the slump that escaped this pillow blanket. What mode of transport conveyed the units to their present location?

Comparison of the elongate ridge outboard of Hualālai with the outer edge of Hilina's mid-slope bench suggests similar emplacement mechanisms for these features. Dimensional and lithologic similarities between the elongate ridge and one of the blocks outboard of the Hilina slump may point to similarity in transport styles. The Hilina block, which was explored in 1998 by *Kaiko* dive K93 (Lipman et al., 2002), apparently detached from an over-steepened slump surface at the foot of the mid-slope bench above it. It measures 4 km × 13 km, rises 400–800 m above the surrounding area, and is also oriented parallel to the shoreline. The steepest part of the slope from which the K93 block calved is ~15°, which is identical to the steepest portion of the slope of the North Kona slump landward of the S692 sliver. The slope between the K93 block and the Hilina mid-slope bench is ~5°, again identical to the average slope between the elongate sliver and the 3000 m contour of the North Kona bench. The K93 block is made up of indurated volcanoclastic materials, mostly glass sandstones and brecciated pillows, just as in the

S692 sliver. The chemical alteration patterns, including intensification of secondary mineralization towards the base, are common to both packages, and probably occurred during incremental slip within their respective slumps. The main difference between the orientations of the K93 block and S692 sliver is that the K93 block is about twice as far (24 km) from its source area as the sliver is from the 3000 m contour of the North Kona slump (13 km).

From the observations and comparisons described above, we conclude that the elongate sliver has a compound history as the product of volcanoclastic accumulation, incremental sliding, and fully detached separation from the foot of the North Kona slump deposit. This interpretation is the simplest physically plausible explanation that is consistent with all bathymetric, lithologic, and petrographic data. The sliver may be the lone remnant of a dense debris field shed to lesser and greater distances from the slump toe. This particular package apparently escaped burial by lava flows because of its separation from the edifice, and avoided remobilization in the 'Ālika 2 avalanche because of its relative proximity. We postulate that Hualālai's flank provides a picture of what Kīlauea's south flank may look like in a few hundred thousand years, if tholeiite lavas and/or debris cover the midslope (Hilina) bench, leaving only the K93 block exposed to provide a record of pre-shield volcanism.

9. History of volcano growth and slumping preserved in the elongate ridge

A goal of this study is to merge inferences drawn from bathymetry data, dive observations, hand sample petrography, and compositional data into a coherent model for the origin, transport and emplacement of the volcanoclastic materials within the elongate ridge studied in dive S692. The following sequence of geologic events traces the development of Hualālai's submarine flank as inferred from the North Kona dive results (Fig. 12).

Alkalic magmas of juvenile Hualālai were generated starting at ~700 k.y.a. (Moore and Clague, 1992) by small extents of partial melting deep in the mantle, consistent with the canonical model of Hawaiian volcano development (Chen and Frey, 1983; Garcia et al., 1989; DePaolo and Stolper, 1996). Thus far, primitive alkalic magmas that would unequivocally represent this period have not been recovered from Hualālai. However, the hawaiitic glassy pillow breccias of samples #4 and #5 may be fractionated representatives of the volcano's earliest shield, possibly formed by clinopyrox-

ene fractionation from primitive melts of tholeiitic affinity. The hawaiites retain high S-contents from quenching at high confining pressure due to eruption into deep (>1 km) water. Alkalic glasses with low S were not recovered, so presently there is no evidence indicating whether Hualālai closely approached or exceeded sea level in this period, as the juvenile Kīlauea apparently did (Coombs et al., 2006-this issue). Reef dating reveals that Hualālai volcano grew on the south flank of Mauna Kea, and exceeded sea level before 300 ka (Moore et al., 1989), giving this as an upper limit for the age of eruption of the hawaiite magma.

Hualālai entered a period of transition during which successive eruptions alternated between tholeiite and transitional basalt, representing a heterogeneous mixture of LREE enrichments. The S-rich glass fragments within pillow breccia samples #11 and #12 and glass sandstone of #7 represent volumetrically minor eruptions from deep-water vents. The volcano grew above sea level and produced degassed tholeiitic magmas having consistently lower LREE enrichments and Mauna Loa-like CaO–MgO values by greater extents of partial melting. Glass fragments, which we infer to have formed by fragmentation at the shoreline, were transported down the flank where they settled out to form a heterogeneous mixture (i.e., composed of products of multiple eruptive events). The angularity of the sandstone fragments indicates that they were probably transported by dilute turbidite currents (Garcia and Hull, 1994). We infer from the compositional variety of the sliver, including alkalic to transitional to tholeiitic basalts compressed in a ~50 m vertical stratigraphic sequence, that these sediments accumulated far (≥ 10 km) from their eruption sites.

Stacks of bedded glass sandstones, submarine and subaerial-erupted lavas and glass-rich pillow breccias were assembled on the flanks in relatively deep water (as required by the few high-S grains within the pillow breccias) but relatively close to lava emplacement depths (as required by coarse breccia grain sizes). For example, we infer that unit IV was emplaced on a slope steep enough to cause the flows (comprising samples #13–15) to tear apart. Units II–V (samples #11–16) are similar to lithologies sampled from Kīlauea's south flank (Lipman et al., 2002), the Wai'anae slump (Coombs et al., 2004a), blocks within the Nu'uānu landslide off Ko'olau (Clague et al., 2002; Yokose, 2002) and the Laupāhoehoe slump off Kohala (Coombs and Kimura, unpublished data).

The accumulated materials representing units I–IV were transported to deep water as a coherent stack.

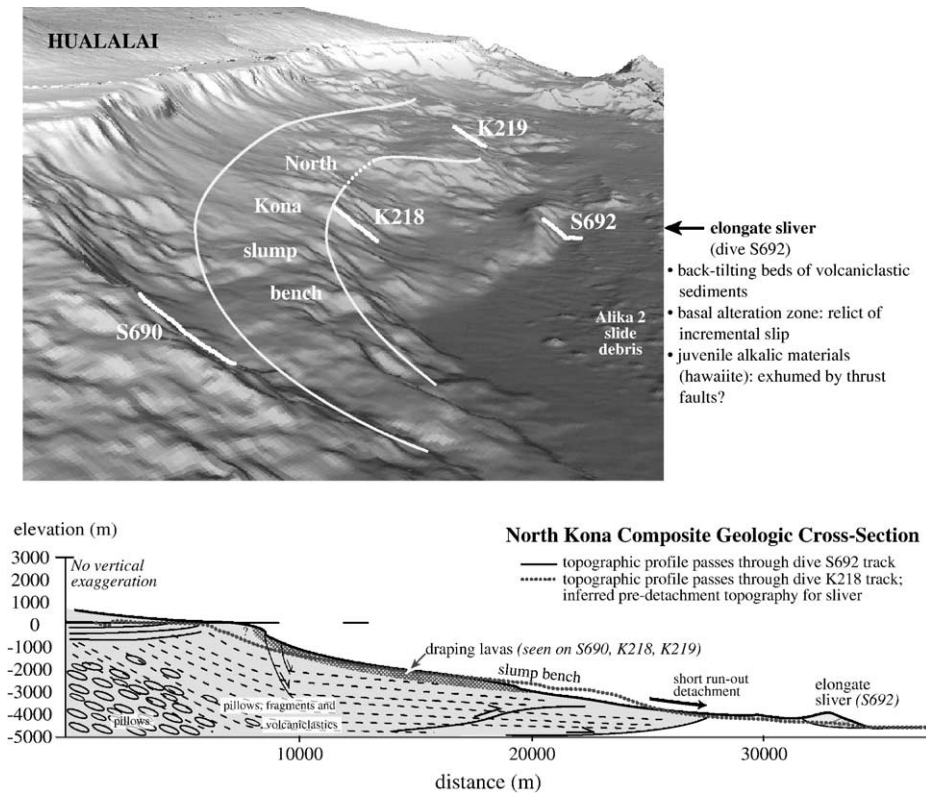


Fig. 12. Perspective view of shaded topography in the submarine North Kona region, looking to the southeast from the western end of Hualālai northwest rift zone. Bottom tracks for dives K218, K219, S690, and S692 are indicated with heavy white lines. Key features include a bench in the North Kona slump deposit (approximately bounded by thin white lines), the eastern edge of the ‘Ālika 2 avalanche field, and the elongate sliver (viewed end-on) described here. Below, a cross-sectional sketch passing through dive S692 perpendicular to Hualālai’s shore line illustrates (1) the surficial materials investigated in this study: draping tholeiitic lavas seen on dives K218, K219, and S690, and the package of volcanoclastic, pillow breccias, and lavas encountered on dive S692, and (2) a highly speculative inferred subsurface geology and structures, based on studies at Hilina (Hills et al., 2002; Lipman et al., 2002), and Mauna Loa (Moore and Chadwick, 1995; Garcia and Davis, 2001).

Several lines of evidence support the assertion that the elongate ridge represents recurrent transport of a detached block by incremental sliding. (A) Intensification of alteration and secondary mineralization along a diffuse zone at the base of the package may indicate this was a pathway for hydrothermal fluids. Whether this was also a zone of deformation cannot be concluded, but comparative studies suggest that such zones accommodate shearing as a load is moved incrementally (Masson et al., 2002; Petley et al., 2002). (B) The basal cauliflower-textured breccia unit is analogous to a horizon observed at the base of the Hilina slump, interpreted as proximal debris-flow breccia deposits from recurrent submarine and shoreline slope failures (Lipman et al., 2002). (C) Mid-level pillow breccias retain puzzle-piece fractures at mm and cm-scales. If these breccias formed at or near shore (as inferred from low S contents), the angularity of clasts require that transport to the present location occurred within a coherent package. (D) Compression in the lower

reaches of a slump enhances compaction and lithification. These points are consistent with a slump-style mass movement of units I–IV down Hualālai flanks. We infer that the materials ultimately composing the elongate ridge were first emplaced at the outer edge of the North Kona slump, near the present-day 3000 m contour.

The over-steepened outer lip of the slump detached and slid as a block to its present position in deep water. Subsequent lavas draped the North Kona slump, seemingly across its full NW–SE extent, as evidenced by observations during dives K218 and K219 (Lipman and Coombs, 2006-this issue). The vents for these flows have not been identified. The detached block represents the lone exposure of volcanoclastic materials that presumably form the core of the prominent bench upslope.

Volcanoclastic sedimentation in deep water capped the block. The layers of unit V are characterized by fine bedding, a high radiolarian concentration, very fine grain size, poor consolidation, diverse componen-

try, and degassed tholeiite glass fragments (Table 3). This unit probably contains reworked materials from lower in the package that were mobilized by the passing debris avalanche (i.e., 'Ālika 2, ~100 k.y.a.), and re-deposited on top. Evidence that Hualālai-erupted materials were entrained in the 'Ālika 2 avalanche includes the presence of low-SiO₂, low-MgO glass fragments dissimilar to Mauna Loa glasses in gravity cores of the 'Ālika 2 debris lobe, which McMurtry et al. (1999) interpreted as having erupted from Hualālai. While the compositions of these grains do not closely match any of the S692 glasses, they are similar to submarine-emplaced post-shield alkalic basalts (Fig. 5).

10. Conclusions

Our examination of the S692 glasses indicates that the transition from alkalic to tholeiitic magmatism may be unsteady, lasting well into the subaerial portion of the shield-building period. The alkalic materials collected from the base of the detached block make Hualālai the first Hawaiian volcano from which early shield alkalic, main-stage shield tholeiitic, and post-shield alkalic samples have been recovered. Although the samples from dive S692 do not constitute a complete evolutionary trend, these findings support the paradigm of Hawaiian volcano progression through an alkalic–tholeiitic–alkalic sequence. Our preliminary assessment of mantle source characteristics through time for Hualālai is that the juvenile alkalic magma source is similar (except for slightly elevated HFSE) to that of early shield stage transitional basalts. The post-shield magmas suggest a role for phlogopite in mantle processes, whereas this signature is absent from the early shield alkalic magmas. Clinopyroxene evidently dominated the melting mode during the formation of the juvenile transitional basalts within the garnet stability field. Fractional crystallization of clinopyroxene also controlled the liquid line of descent along which hawaiitic magmas evolved, suggesting early development of a deep-seated magmatic reservoir at Hualālai. These early shield alkalic liquids are highly differentiated, and may have derived from transitional-affinity (rather than alkalic) parent magmas by crystal fractionation at moderately high pressure.

The submarine dives S690, K218, and K219 all encountered compositionally similar tholeiite lavas representing Hualālai's main shield stage of development. These draping lavas are more recent than the formation of the North Kona slump bench, which must have started to develop prior to the peak of

shield building (Lipman and Coombs, 2006-this issue). Unless these dives encountered a small number of sparse flows purely by coincidence, we can infer that such lavas blanket much of the bench. Only the elongate sliver of volcanoclastic materials studied on dive S692 presents tangible evidence of the volcano's juvenile magmatic stage, bench lithology (including both deep-water and shallow-erupted volcanoclastics), and recurrent landsliding that accompanied flank development. The sliver escaped burial because it is apparently out of reach of lavas issuing from either now-submerged submarine rift zones or radial volcanic vents. Relatively recent truncation of the sliver by the passage of the 'Ālika 2 avalanche fortuitously provided outcrop exposures suitable for examination and sampling by submersible.

Acknowledgments

We thank Captain Tanaka of the *R.V. Yokosuka*, the submersible teams and marine crews, and the chief scientist E. Takahashi for the opportunity to participate in the JAMSTEC Hawaii cruises. Thanks also to the scientific parties, particularly H. Yokose for assistance in dive site selection during the 2002 cruise and Mike Coffin as the observer for dive S690. We are grateful for discussions with Simon Day, Michael Garcia, and Julia Morgan. Insightful reviews by David Clague, Brian Cousens, Fred Frey, Peter Lipman, and Tom Sisson are much appreciated. This work was supported by the USGS Volcano Hazards Program, an NWS Research Fellowship to Shamberger at the University of Hawaii, and NSF award EAR-0236564.

References

- Anonymous, 1981. Oceanic intraplate volcanism. In: Kaula, W.M. (Ed.), *Basaltic Volcanism on the Terrestrial Planets*. Pergamon Press, New York, pp. 161–192.
- Bohrson, W.A., Clague, D.A., 1988. Origin of ultramafic xenoliths containing exsolved pyroxenes from Hualālai volcano, Hawaii. *Contributions to Mineralogy and Petrology* 100 (2), 139–155.
- Chen, C.-Y., Frey, F.A., 1983. Origin of Hawaiian tholeiite and alkalic basalt. *Nature (London)* 302 (5911), 785–789.
- Chipera, S.J., Apps, J.A., 2001. Geochemical stability of natural zeolites. In: Bish, D.L., Ming, D.W. (Eds.), *Natural Zeolites: Occurrence, Properties, and Applications*, pp. 117–157.
- Clague, D.A., 1982. Petrology of tholeiitic basalt dredged from Hualālai volcano. *EOS Transactions American Geophysical Union* 64, 902.
- Clague, D.A., Frey, F.A., 1982. Petrology and trace element geochemistry of the Honolulu volcanics, O'ahu; implications for the oceanic mantle below Hawaii. *Journal of Petrology* 23 (3), 447–504.
- Clague, D.A., Moore, J.G., 1991. Geology and petrology of Māhukona volcano, Hawaii. *Bulletin of Volcanology* 53 (3), 159–172.

- Clague, D., Jackson, E.D., Wright, T.L., 1980. Petrology of Hualālai volcano, Hawaii: implications for mantle composition. *Bulletin of Volcanologie* 43 (4), 641–656.
- Clague, D.A., Fitton, J.G., Upton, B.G.J., 1987. Hawaiian alkaline volcanism. *Alkaline Igneous Rocks* 30, 227–252.
- Clague, D.A., Davis, A.S., Bischoff, J.L., Dixon, J.E., Geyer, R., 2000. Lava bubble-wall fragments formed by submarine hydro-volcanic: explosions on Lō'ihī seamount and Kīlauea volcano. *Bulletin of Volcanology* 61 (7), 437–449.
- Clague, D., Moore, J.G., Davis, A.S., 2002. Volcanic breccia and hyaloclastite in blocks from the Nu'uānu and Wailau landslides, Hawaii. In: Takahashi, E., Lipman, P.W., Garcia, M.O., Naka, J., Aramaki, S. (Eds.), *Hawaiian Volcanoes: Deep Underwater Perspectives*. AGU, Washington, D.C., pp. 279–296.
- Class, C., Goldstein, S.L., 1997. Plume–lithosphere interactions in the ocean basins: constraints from the source mineralogy. *Earth and Planetary Science Letters* 150 (3–4), 245–260.
- Cohen, A.S., Onions, R.K., Kurz, M.D., 1996. Chemical and isotopic variations in Mauna Loa tholeiites. *Earth and Planetary Science Letters* 143 (1–4), 111–124.
- Coombs, M.L., Clague, D.A., Moore, G.F., Cousens, B.L., 2004a. The growth and collapse of Wai'ānae volcano, Hawaii, as revealed by exploration of its submarine flanks. *Geochemistry, Geophysics, Geosystems* 5 (8). doi:10.1029/2004GC000717.
- Coombs, M.L., Sisson, T.W., Kimura, J.I., 2004b. Ultra-high chlorine in submarine Kīlauea glasses: evidence for direct assimilation of brine by magma. *Earth and Planetary Science Letters* 217, 297–313.
- Coombs, M.L., Sisson, T.W., Lipman, P.W., 2006. Growth history of Kīlauea inferred from volatile-based eruption depths. *Journal of Volcanology and Geothermal Research* 151, 19–49. doi:10.1016/j.jvolgeores.2005.07.037 (this issue).
- Cousens, B.L., Clague, D.A., Sharp, W.D., 2003. Chronology, chemistry, and origin of trachytes from Hualālai volcano, Hawaii. *Geochemistry, Geophysics, Geosystems* 4, 1078. doi:10.1029/2003GC000560.
- Davis, M.G., Garcia, M.O., Wallace, P., 2003. Volatiles in glasses from Mauna Loa volcano, Hawaii: implications for magma degassing and contamination, and growth of Hawaiian volcanoes. *Contributions to Mineralogy and Petrology* 144 (5), 570–591.
- DePaolo, D.J., Stolper, E.M., 1996. Models of Hawaiian volcano growth and plume structure: implications of results from the Hawaii Scientific Drilling Project. *Journal of Geophysical Research-Solid Earth* 101 (B5), 11643–11654.
- Dixon, J.E., Clague, D.A., Stolper, E.M., 1991. Degassing history of water, sulfur, and carbon in submarine lavas from Kīlauea volcano, Hawaii. *Journal of Geology* 99 (3), 371–394.
- Elsworth, D., Day, S.J., 1999. Flank collapse triggered by intrusion: the Canary and Cape Verde archipelagos. *Journal of Volcanology and Geothermal Research* 94 (1–4), 323–340.
- Frey, F.A., Clague, D.A., 1983. Geochemistry of diverse basalt types from seamount, Hawaii; petrogenetic implications. *Earth and Planetary Science Letters* 66, 337–355.
- Frey, F.A., Rhodes, J.M., 1993. Intershield geochemical differences among Hawaiian volcanoes: implications for source compositions, melting processes and magma ascent paths. *Philosophical Transactions of the Royal Society of London*. A 342, 121–136.
- Frey, F.A., Wise, W.S., Garcia, M.O., West, H., Kwon, S.T., Kennedy, A., 1990. Evolution of Mauna Kea volcano, Hawaii—petrologic and geochemical constraints on postshield volcanism. *Journal of Geophysical Research-Solid Earth and Planets* 95 (B2), 1271–1300.
- Frey, F.A., Garcia, M.O., Wise, W.S., Kennedy, A., Gurriet, P., Albarede, F., 1991. The evolution of Mauna Kea volcano, Hawaii—petrogenesis of tholeiitic and alkalic basalts. *Journal of Geophysical Research-Solid Earth and Planets* 96 (B9), 14347–14375.
- Fujimaki, H., Tatsumoto, M., Aoki, K., 1984. Partition coefficients of Hf, Zr, and REE between phenocrysts and groundmasses. *Journal of Geophysical Research* 89, B662–B672.
- Furnes, H., Staudigel, H., Thorseth, I.H., Torsvik, T., Muehlenbachs, K., Tummy, O., 2001. Bioalteration of basaltic glass in the oceanic crust. *Geochemistry, Geophysics, Geosystems* 2 (2000GC000150).
- Garcia, M.O., Davis, M.G., 2001. Submarine growth and internal structure of ocean island volcanoes based on submarine observations of Mauna Loa volcano Hawaii. *Geology* 29 (2), 163–166.
- Garcia, M.O., Hull, D.M., 1994. Turbidites from giant Hawaiian landslides—results from Ocean Drilling Program site-842. *Geology* 22 (2), 159–162.
- Garcia, M.O., Muenow, D.W., Aggrey, K.E., Oneil, J.R., 1989. Major element, volatile, and stable isotope geochemistry of Hawaiian submarine tholeiitic glasses. *Journal of Geophysical Research-Solid Earth and Planets* 94 (B8), 10525–10538.
- Garcia, M.O., Rhodes, J.M., Wolfe, E.W., Ulrich, G.E., Ho, R.A., 1992. Petrology of lavas from episodes 2–47 of the Pu'u 'Ō'ō eruption of Kīlauea volcano, Hawaii—evaluation of magmatic processes. *Bulletin of Volcanology* 55 (1–2), 1–16.
- Garcia, M.O., Jorgenson, B.A., Mahoney, J.J., Ito, E., Irving, A.J., 1993. An evaluation of temporal geochemical evolution of Lō'ihī summit lavas—results from Alvin submersible dives. *Journal of Geophysical Research-Solid Earth* 98 (B1), 537–550.
- Garcia, M.O., Foss, D.J.P., West, H.B., Mahoney, J.J., 1995. Geochemical and isotopic evolution of Lō'ihī volcano Hawaii. *Journal of Petrology* 36 (6), 1647–1674.
- Gurriet, P.C., 1988. *Geochemistry of Hawaiian dredged lavas*. MSc Thesis, MIT, Cambridge, 177 pp.
- Hills, D.J., Morgan, J.K., Moore, G., Leslie, S., 2002. Structural variability along the submarine south flank of Kīlauea volcano, Hawaii, from a multichannel seismic reflection survey. In: Takahashi, E., Lipman, P.W., Garcia, M.O., Naka, J., Aramaki, S. (Eds.), *Hawaiian Volcanoes: Deep Underwater Perspectives*. AGU, Washington, D.C., pp. 105–124.
- Hofmann, A., 1997. *Mantle geochemistry: the message from oceanic volcanism*. *Nature* 385, 219–229.
- Hofmann, A.W., 1988. Chemical differentiation of the earth—the relationship between mantle, continental-crust, and oceanic-crust. *Earth and Planetary Science Letters* 90 (3), 297–314.
- Hofmann, A.W., Jochum, K.P., 1996. Source characteristics derived from very incompatible trace elements in Mauna Loa and Mauna Kea basalts, Hawaii Scientific Drilling Project. *Journal of Geophysical Research, B, Solid Earth and Planets* 101, 11831–11839.
- Huang, S., Frey, F.A., 2003. Trace element abundances of Mauna Kea basalt from phase 2 of the Hawaii Scientific Drilling Project: petrogenetic implications of correlations with major element content and isotopic ratios. *Geochemistry Geophysics* 4.
- Irvine, T.N., Baragar, W.R.A., 1971. A guide to the chemical classification of the common volcanic rocks. *Canadian Journal of Earth Sciences* 8, 523–548.
- Kauahikaua, J., Cashman, K.V., Clague, D.A., Champion, D., Hagstrum, J.T., 2002. Emplacement of the most recent lava flows on Hualālai volcano Hawaii. *Bulletin of Volcanology* 64 (3–4), 229–253.

- Kurz, M.D., Kenna, T.C., Kammer, D.P., Rhodes, J.M., Garcia, M.O., 1995. Isotopic evolution of Mauna Loa volcano: a view from the submarine southwest rift zone. In: Rhodes, J.M., Lockwood, J.P. (Eds.), *Mauna Loa Revealed: Structure, Composition, History, and Hazards*. Geophysical Monograph Series. AGU, Washington, D.C., pp. 289–306.
- Kushiro, I., 1969. The system forsterite–diopside–silica with and without water at high pressures. *American Journal of Science* 267-A, 269–294.
- Le Maitre, R.W., 2002. *Igneous Rocks: A Classification and Glossary of Terms*. Cambridge University Press, Cambridge. 236 pp.
- Lipman, P.W., 1980. The southwest rift zone of Mauna Loa: implications for structural evolution of Hawaiian volcanoes. *American Journal of Science* 280-A, 752–776.
- Lipman, P.W., Coombs, M.L., 2006. Submarine slumping on the north kona flank of Hualalai volcano (Hawaii) during tholeiitic shield-stage volcanism. *Journal of Volcanology and Geothermal Research* 151, 189–216. doi:10.1016/j.jvolgeores.2005.07.029 (this issue).
- Lipman, P.W., Normark, W.R., Moore, J.G., Wilson, J.B., Gutmacher, C.E., 1988. The giant submarine ‘Ālika debris-slide, Mauna Loa, Hawaii. *Journal of Geophysical Research-Solid Earth and Planets* 93 (B5), 4279–4299.
- Lipman, P.W., Sisson, T.W., Ui, T., Naka, J., 2000. In search of ancestral Kīlauea volcano. *Geology* 28 (12), 1079–1082.
- Lipman, P., Sisson, T.W., Ui, T., Naka, J., Smith, J.R., 2002. Ancestral submarine growth of Kīlauea volcano and instability of its south flank. In: Takahashi, E., Lipman, P.W., Garcia, M.O., Naka, J., Aramaki, S. (Eds.), *Hawaiian Volcanoes: Deep Underwater Perspectives*. Geophysical Monograph Series. AGU, Washington, D.C., pp. 161–192.
- Macdonald, G.A., 1968. Composition and origin of Hawaiian lavas. *Memoir - Geological Society of America* 116, 477–522.
- Macdonald, G.A., Katsura, T., 1964. Chemical composition of Hawaiian lavas. *Journal of Petrology* 5, 82–133.
- Mahood, G.A., Baker, D.R., 1986. Experimental constraints on depths of fractionation of mildly alkalic basalts and associated felsic rocks: Pantelleria, strait of Sicily. *Contributions to Mineralogy and Petrology* 93, 251–264.
- Masson, D.G., Urgeles, R., Mitchell, N.C., Le Bas, T.P., Canals, M., Watts, A.B., Gee, M.J.R., 2002. Slope failures on the flanks of the western canary islands. *Earth-Science Reviews* 57 (1–2), 1–35.
- Masuda, Y., Yagi, S., Asayama, T., 1974. Instrumental neutron activation analysis of 13 trace elements in volcanic rocks. *Bulletin of the University of Osaka Prefecture* 23, 203–213.
- McDonough, W.F., Sun, S.S., 1995. The composition of the earth. *Chemical Geology* 120 (3–4), 223–253.
- McMurtry, G.M., Herrero-Bervera, E., Cremer, M.D., Smith, J.R., Resig, J., Sherman, C., Torresan, M.E., 1999. Stratigraphic constraints on the timing and emplacement of the ‘Ālika 2 giant Hawaiian submarine landslide. *Journal of Volcanology and Geothermal Research* 94 (1–4), 35–58.
- McMurtry, G.M., Watts, P., Fryer, G.J., Smith, J.R., Imamura, F., 2004. Giant landslides, mega-tsunamis, and paleo-sea level in the Hawaiian islands. *Marine Geology* 203, 219–233.
- Moore, R.B., 1987. Unpublished data. The Bishop Museum.
- Moore, J.G., Chadwick, W.W.J., 1995. Offshore geology of Mauna Loa and adjacent areas, Hawaii. In: Rhodes, J.M., Lockwood, J.P. (Eds.), *Mauna Loa Revealed: Structure, Composition, History, and Hazards*. Geophysical Monograph Series. AGU, Washington, D.C., pp. 21–44.
- Moore, J.G., Clague, D.A., 1987. Coastal lava flows from Mauna Loa and Hualālai volcanoes, Kona, Hawaii. *Bulletin of Volcanology* 49 (6), 752–764.
- Moore, J.G., Clague, D.A., 1992. Volcano growth and evolution of the island of Hawaii. *Geological Society of America Bulletin* 104 (11), 1471–1484.
- Moore, J.G., Fabbri, B.P., 1971. An estimate of the juvenile sulfur content of basalt. *Contributions to Mineralogy and Petrology* 33, 118–127.
- Moore, J.G., Clague, D.A., Normark, W.R., 1982. Diverse basalt types from Lō‘ihi seamount, Hawaii. *Geology (Boulder)* 10 (2), 88–92.
- Moore, R.B., Clague, D., Rubin, M., Bohrsen, W.A., 1987. Hualālai volcano: a preliminary summary of geologic, petrologic, and geophysical data. In: Decker, R.W., Wright, T.L., Stauffer, P.H. (Eds.), *U. S. Geological Survey Professional Paper*, vol. 1350. U.S. Govt. Printing Office, Washington, D.C., pp. 1527–1567.
- Moore, J.G., Clague, D.A., Holcomb, R.T., Lipman, P.W., Normark, W.R., Torresan, M.E., 1989. Prodigious submarine landslides on the Hawaiian ridge. *Journal of Geophysical Research, B, Solid Earth and Planets* 94 (12), 17,465–17,484.
- Moore, J.G., Normark, W.R., Holcomb, R.T., 1994. Giant Hawaiian landslides. *Annual Review of Earth and Planetary Sciences* 22, 119–144.
- Morgan, J.K., Moore, G.F., Hills, D.J., Leslie, S., 2000. Overthrusting and sediment accretion along Kīlauea’s mobile south flank, Hawaii: evidence for volcanic spreading from marine seismic reflection. *Geology* 28 (7), 667–670.
- Naka, J., 2002. Introduction to section 1. In: Takahashi, E., Lipman, P.W., Garcia, M.O., Naka, J., Aramaki, S. (Eds.), *Hawaiian Volcanoes: Deep Underwater Perspectives*. Geophysical Monograph Series, AGU, Washington, D.C., pp. 1–2.
- Naumann, T.R., Geist, D.J., 1999. Generation of alkalic basalt by crystal fractionation of tholeiitic magma. *Geology* 27 (5), 423–426.
- Norman, M.D., Garcia, M.O., 1999. Primitive magmas and source characteristics of the Hawaiian plume: petrology and geochemistry of shield picrites. *Earth and Planetary Science Letters* 168 (1–2), 27–44.
- Norman, M.D., Garcia, M.O., Kamenetsky, V.S., Nielsen, R.L., 2002. Olivine-hosted melt inclusions in Hawaiian picrites: equilibration, melting, and plume source characteristics. *Chemical Geology* 183 (1–4), 143–168.
- O’Hara, M.J., 1968. The bearing of phase equilibria studies in synthetic and natural systems on the origin and evolution of basic and ultrabasic rocks. *Earth-Science Reviews* 4, 69–133.
- Petley, D.N., Bulmer, M.H., Murphy, W., 2002. Patterns of movement in rotational and translational landslides. *Geology* 30 (8), 719–722.
- Presley, T.K., Sinton, J.M., Pringle, M., 1997. Postshield volcanism and catastrophic mass wasting of the Waianae volcano, O’ahu, Hawaii. *Bulletin of Volcanology* 58 (8), 597–616.
- Reed, S.J.B., 1993. *Electron Microprobe Analysis*. Cambridge University Press, Cambridge. 326 pp.
- Rhodes, J.M., 1996. Geochemical stratigraphy of lava flows sampled by the Hawaii Scientific Drilling Project. *Journal of Geophysical Research-Solid Earth* 101 (B5), 11729–11746.
- Rhodes, J.M., Hart, S.R., 1995. Episodic trace element and isotopic variations in historical Mauna Loa lavas: implications for magma and plume dynamics. In: Rhodes, J.M., Lockwood, J.P. (Eds.), *Mauna Loa Revealed: Structure, Composition, History, and Hazards*. Geophysical Monograph Series, American Geophysical Union, Washington, D.C., pp. 263–288.

- Rhodes, J.M., Vollinger, M.J., 2004. Composition of basaltic lavas sampled by phase-2 of the Hawaii Scientific Drilling Project: geochemical stratigraphy and magma types. *Geochemistry Geophysics* 5.
- Roeder, P.L., Emslie, R.F., 1970. Olivine-liquid equilibrium. *Contributions to Mineralogy and Petrology* 29, 275–289.
- Ryan, M.P., 1979. The cyclic elastic-plastic fracture mechanics of subsolidus Hawaiian olivine tholeiite. In: Decker Robert, W., Drake, C., Eaton, G., Hellsley, C. (Eds.), *Hawaii Symposium on Intraplate Volcanism and Submarine Volcanism*; abstract volume. U.S. Geological Survey, vol. 147. Hawaiian Volcano Observatory, Hawaii National Park, HI.
- Sack, R.O., Walker, D., Carmichael, I.S.E., 1987. Experimental petrology of alkalic lavas: constraints on cotectics of multiple saturation in natural basic liquids. *Contributions to Mineralogy and Petrology* 96, 1–23.
- Schiffman, P., Walton, A., 2003. Alteration of hyaloclastites in the hsdp 2 phase 1 drill core: 1. Description and paragenesis. *GSA Today* 4 (5). doi:10.1029/2002GC000368.
- Siems, D.F., 2000. The determination of 30 elements in geologic materials by energy-dispersive X-ray fluorescence spectrometry. Open-File Report, U. S. Geological Survey, 13.
- Sims, K.W.W., DePaolo, D.J., Murrell, M.T., Baldrige, W.S., Goldstein, S.J., Clague, D.A., 1995. Mechanisms of magma generation beneath Hawaii and mid-ocean ridges; uranium/thorium and samarium/neodymium isotopic evidence. *Science* 267 (5197), 508–512.
- Sims, K.W.W., DePaolo, D.J., Murrell, M.T., Baldrige, W.S., Goldstein, S., Clague, D., Jull, M., 1999. Porosity of the melting zone and variations in the solid mantle upwelling rate beneath Hawaii: inferences from U-238–Th-230–Ra-226 and U-235–Pa-231 disequilibria. *Geochimica et Cosmochimica Acta* 63 (23–24), 4119–4138.
- Sisson, T.W., Lipman, P.W., Naka, J., 2002. Submarine alkalic through tholeiitic shield-stage development of Kīlauea volcano, Hawaii. In: Takahashi, E., Lipman, P.W., Garcia, M.O., Naka, J., Aramaki, S. (Eds.), *Hawaiian Volcanoes: Deep Underwater Perspectives*. Geophysical Monograph Series, AGU, Washington, D.C., pp. 193–220.
- Smith, A.R., Satake, K., Suyehiro, K., 2002. Deepwater multibeam sonar surveys along the southeastern Hawaii ridge: guide to the CD-ROM. In: Takahashi, E., Lipman, P.W., Garcia, M.O., Naka, J., Aramaki, S. (Eds.), *Hawaiian Volcanoes: Deep Underwater Perspectives*. AGU, Washington, D.C., pp. 3–10.
- Sobolev, A.V., Kamenetsky, V.S., Metrich, N., Clocchiatti, R., Kononkova, N.N., Devirts, A.L., Ustinov, V.I., 1990. Regime of volatile components and conditions of crystallization of hawaiite lavas of Etna volcano, Sicily. *Geokhimiya* (9), 1277–1290.
- Stakes, D.S., Shervais, J.W., Hopson, C.A., 1984. The volcano-tectonic cycle of the Famous and Amar valleys, mid-Atlantic ridge (36°47'N): evidence from basalt glass and phenocryst compositional variations for a steady state magma chamber beneath the valley midsections, Amars. *Journal of Geophysical Research* 89, 6995–7028.
- Stearns, H.T., Macdonald, G.A., 1946. Geology and groundwater resources of the island of Hawaii. *Bulletin*, vol. 9. Hawaii Division of Hydrography, Honolulu, p. 363.
- Taggart, J.E., Lindsay, J.R., Scott, B.A., Vivit, D.V., Bartel, A.J., Stewart, K.C., 1987. Analysis of geologic materials by wavelength-dispersive X-ray fluorescence spectrometry. In: Baedecker, P.A. (Ed.), *U. S. Geological Survey Professional Paper*, vol. 1770. pp. E1–E19.
- Tatsumoto, M., 1966. Isotopic composition of lead in volcanic rocks from Hawaii, Iwo Jima, and Japan. *Journal of Geophysical Research* 71 (6), 1721–1733.
- Thorner, C.R., Heliker, C., Sherrod, D.R., Kauahikaua, J.P., Miklius, A., Okubo, P.G., Trusdell, F.A., Budahn, J.R., Ridley, W.I., Meeker, G.P., 2003. Kīlauea east rift zone magmatism: an episode 54 perspective. *Journal of Petrology* 44 (9), 1525–1559.
- Wallace, P., Carmichael, I.S.E., 1992. Sulfur in basaltic magmas. *Geochimica et Cosmochimica Acta* 56 (5), 1863–1874.
- Wanless, V.D., Garcia, M.O., Rhodes, J.M., Weis, D., Norman, M.D., 2006. Shield stage alkalic volcanism on Mauna Loa, Hawaii. *Journal of Volcanology and Geothermal Research* 151, 141–155. doi:10.1016/j.jvolgeores.2005.07.027 (this issue).
- Ward, S.N., 2001. Landslide tsunami. *Journal of Geophysical Research-Solid Earth* 106 (B6), 11201–11215.
- West, H.B., Garcia, M.O., Frey, F.A., Kennedy, A., 1988. Nature and cause of compositional variation among the alkalic cap lavas of Mauna Kea volcano, Hawaii. *Contributions to Mineralogy and Petrology* 100 (3), 383–397.
- Wilson, S.A., Taggart, J.E., 2000. Development of USGS microbeam reference materials for geochemical analysis. *Geoanalysis 2000*. International Association of Geoanalysts, Nancy, France.
- Wolfe, E.W., Morris, J.D., 1996. Geologic map of the island of Hawai'i. U. S. Geological Survey Miscellaneous Investigations Map, I-2524.
- Wolfe, E.W., Wise, W.S., Dalrymple, G.B., 1997. The Geology and Petrology of Mauna Kea Volcano, Hawaii—a Study of Postshield Volcanism. U.S. Govt. Printing Office, Washington, D.C. 129 pp.
- Yang, H.J., Frey, F.A., Garcia, M.O., Clague, D.A., 1994. Submarine lavas from Mauna Kea volcano, Hawaii—implications for Hawaiian shield stage processes. *Journal of Geophysical Research-Solid Earth* 99 (B8), 15577–15594.
- Yoder, H.S., Tilley, C.E., 1962. Origin of basalt magmas: an experimental study of natural and synthetic rock systems. *Journal of Petrology* 3, 342–532.
- Yokose, H., 2002. Landslides on the windward flanks of O'ahu and Molokai, Hawaii: shinkai 6500 submersible investigation. In: Takahashi, E., Lipman, P.W., Garcia, M.O., Naka, J., Aramaki, S. (Eds.), *Hawaiian Volcanoes: Deep Underwater Perspectives*. AGU, Washington, D.C., pp. 245–262.